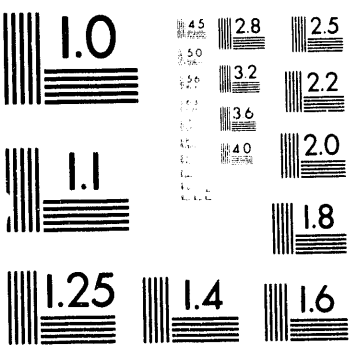
1.0
1.1
1.25
1.4
1.6
1.8
2.0
2.2
2.5
2.8
3.2
3.6
4.0
4.5
5.0

1 of 1

Distribution
Category UC-706

SAND93-0218
Unlimited Release
Printed July 1993

Mission Hazard Assessment for STARS Mission 1 (M1) in the Marshall Islands Area

David E. Outka
Robert A. LaFarge

Flight Dynamics Department
Sandia National Laboratories
Albuquerque, New Mexico 87185

Abstract

A mission hazard assessment has been performed for the Strategic Target System Mission 1 (known as STARS M1) for hazards due to potential debris impact in the Marshall Islands area. The work was performed at Sandia National Laboratories as a result of discussions with Kwajalein Missile Range (KMR) safety officers. The STARS M1 rocket will be launched from the Kauai Test Facility (KTF), Hawaii, and deliver two payloads to within the viewing range of sensors located on the Kwajalein Atoll. The purpose of this work has been to estimate upper bounds for expected casualty rates and impact probability for the Marshall Islands areas which adjoin the STARS M1 instantaneous impact point (IIP) trace. This report documents the methodology and results of the analysis.

The work described in this report was conducted under case number 1751.500 during the months of April through December, 1991. Originally distributed as a memo to the ranges in the Spring of 1992, the current SAND report version differs primarily in format.

Table of Contents

List of Figures

List of Tables

The STARS M1 Hazard Assessment

The STARS Mission 1 (known as STARS M1) is planned to carry two Strategic Defense payloads from the Kauai Test Facility (KTF) to the Marshall Islands area. The terminal portions of the payload trajectories will be observed from various sensor platforms on Kwajalein Atoll and the surrounding area. Primary flight safety responsibility for the mission is assigned to the Naval Air Warfare Center (NAWC), Weapons Division, with cooperation of the Pacific Missile Range Facility (PMRF) and the Kwajalein Missile Range (KMR). Sandia National Laboratories is tasked to provide supporting data and analysis, as requested by the ranges.

As part of this support, a STARS M1 mission hazard assessment has been performed for hazards due to potential debris impact in the Marshall Islands area. The need for this work was recognized following discussions with Kwajalein Missile Range (KMR) safety officers. The objective of the hazard assessment was to estimate upper bounds for expected casualty rates and impact probability for the Marshall Islands areas which adjoin the STARS M1 instantaneous impact point (IIP) trace. This report documents the methodology and results of the hazard analysis.

To keep the IIP well away from inhabited areas, a dogleg maneuver is performed late in the burn of the third stage. This maneuver causes the IIP to approach Kwajalein Atoll from the north, through the widest available corridor (Figure 1). Even so, the software KMR intended to use to perform a real-time safety assessment indicated that the mission could not be performed as planned. However, the real-time software did not provide any information on the probability of a hazardous event actually occurring. Nor was the fact that there were very few people and very little land area in comparison to the large amount of ocean area considered. Simple calculations could be performed which showed that the number of debris impacts per unit area were likely to be extremely low over the areas of concern. A more rigorous treatment of the subject would lay to rest concerns that the simple calculations did not cover all worst case possibilities.

It was known that TRW provided probabilistic hazard assessments in support of Minuteman launches from Vandenburg Air Force Base to KMR, but neither KMR nor Sandia had experience with true probabilistic hazard assessments for rocket missions. Since it appeared that support from TRW would be unfeasible, it was proposed to KMR that Sandia perform a mission hazard assessment for the STARS M1 flight. The intent of this work has been to estimate upper bounds for expected casualty rates and impact probability for the Marshall Islands areas which adjoin the STARS M1 IIP ground track. It is anticipated that this information will assist KMR in making a judgement as to the hazards associated with the mission. In addition to hazards to people on the ground, this data should be useful in estimating the hazards to aircraft, to shipping, and to ground-based assets such as radar equipment.

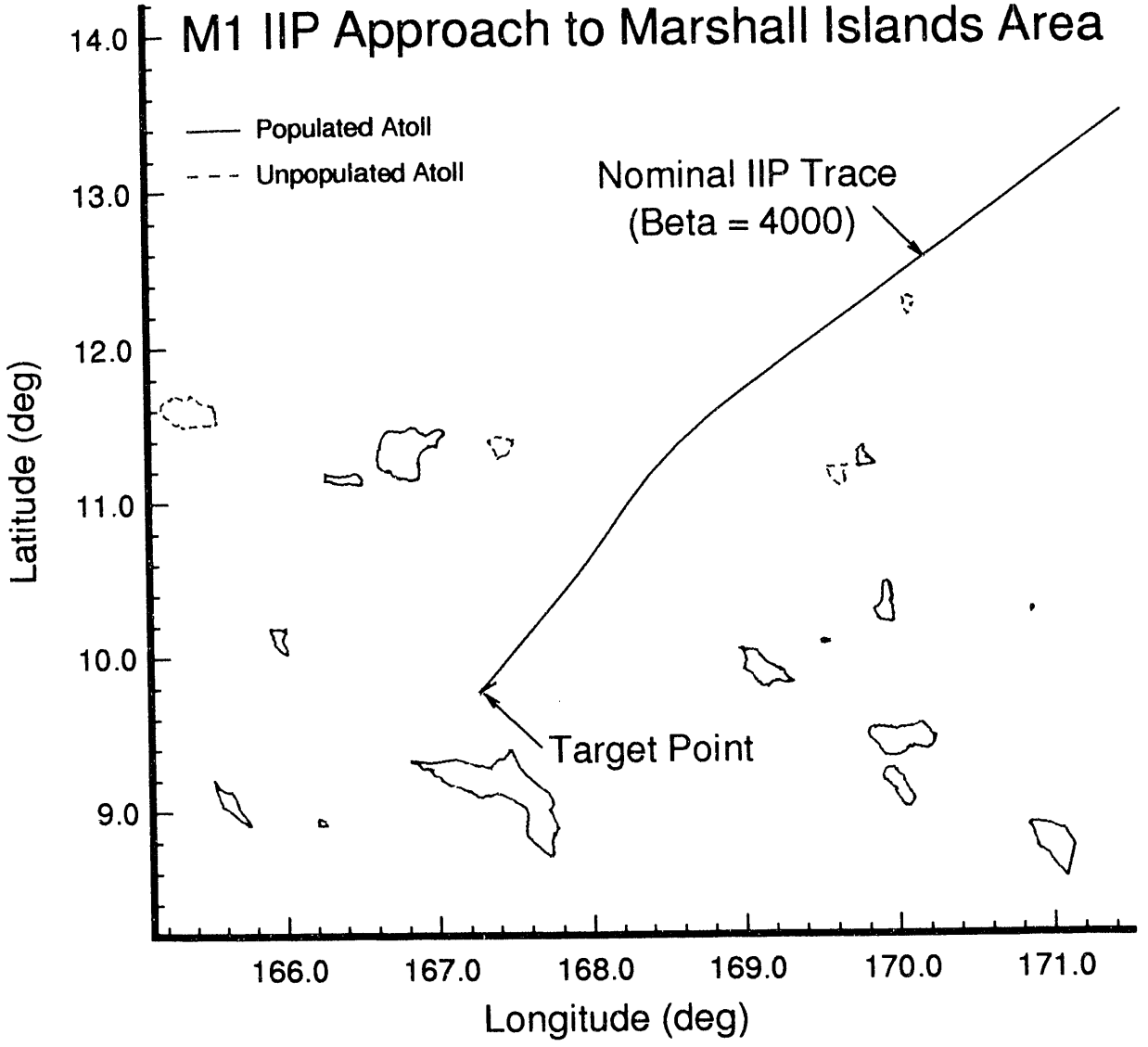

Figure 1: STARS M1 Approaches Kwajalein Through the Corridor to the North

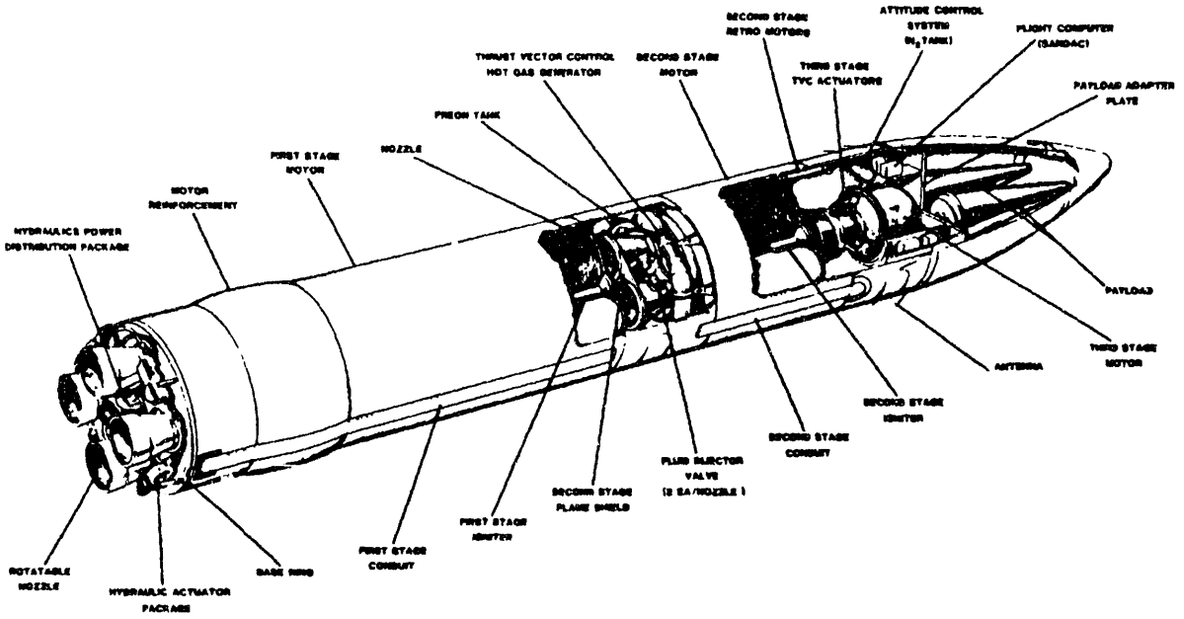

Figure 2: The STARS Vehicle

The STARS Vehicle

The STARS vehicle consists of three stages (Figure 2). The first two stages are derived from retired Polaris A3 fleet ballistic missile assets. Since only the third stage and its payloads reach the Marshall Islands area, the first two stages are not considered in this report. The third stage (Figure 3) is an all new Sandia design, added to meet the objectives of the program. The STARS Orbus 1 third stage motor, shown in Figure 4, was designed and built to Sandia specifications by the Chemical Systems Division of United Technologies Corporation.

Overview of the Analysis Process

The analysis process begins with a failure mode analysis. The components whose failure could cause a flight safety hazard in the form of a trajectory deviation are identified and the failure rate of each of these components is determined. Next, the nature of the trajectory deviation resulting from each specific component failure is identified, permitting the effects of some failure modes to be combined. For example, the third stage nozzle might become fixed in a given position due either to some sort of mechanical failure or to a faulty electrical signal; the effect on the trajectory would be the same in either case.

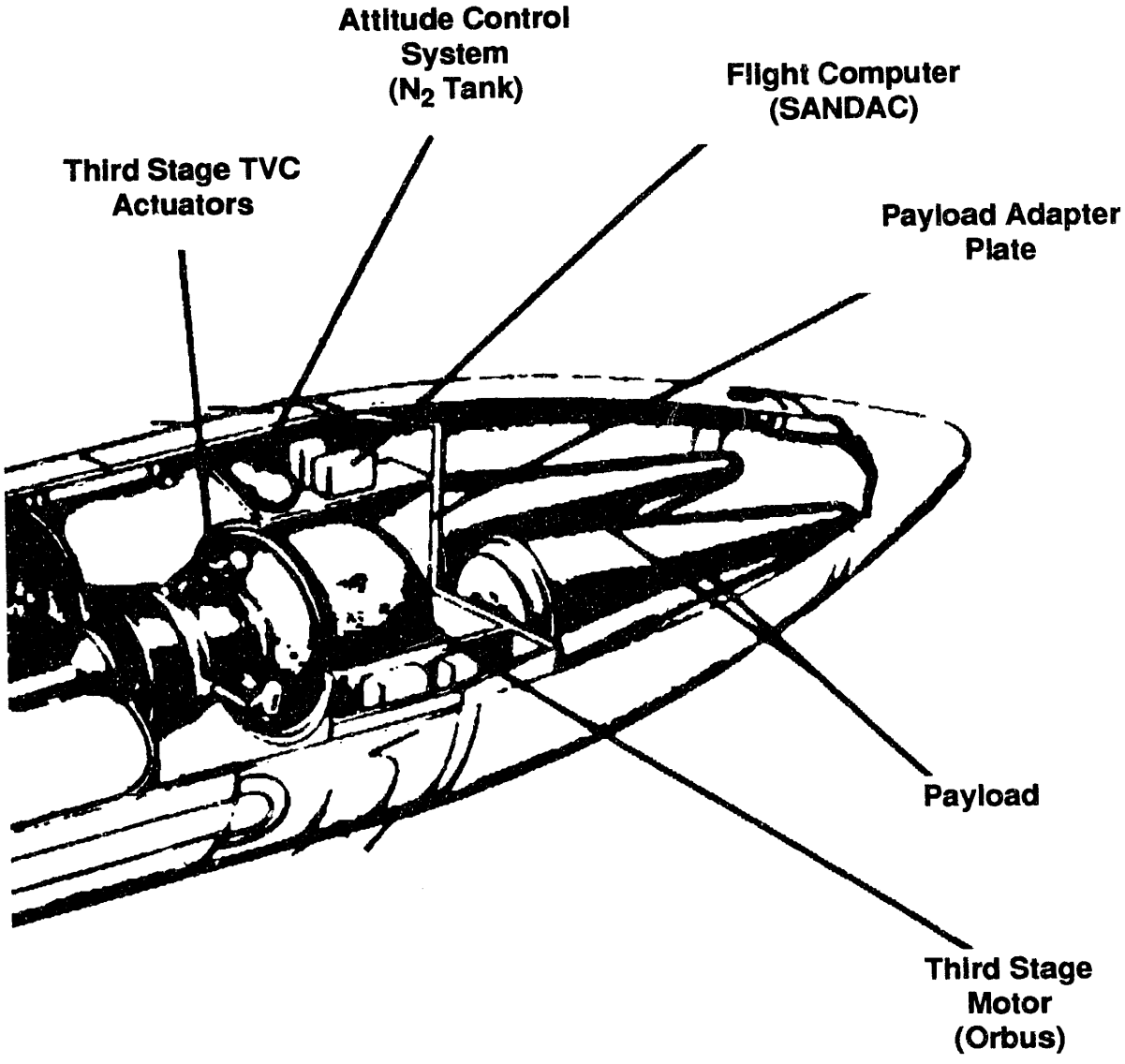

Figure 3: The STARS Third Stage in Launch Configuration

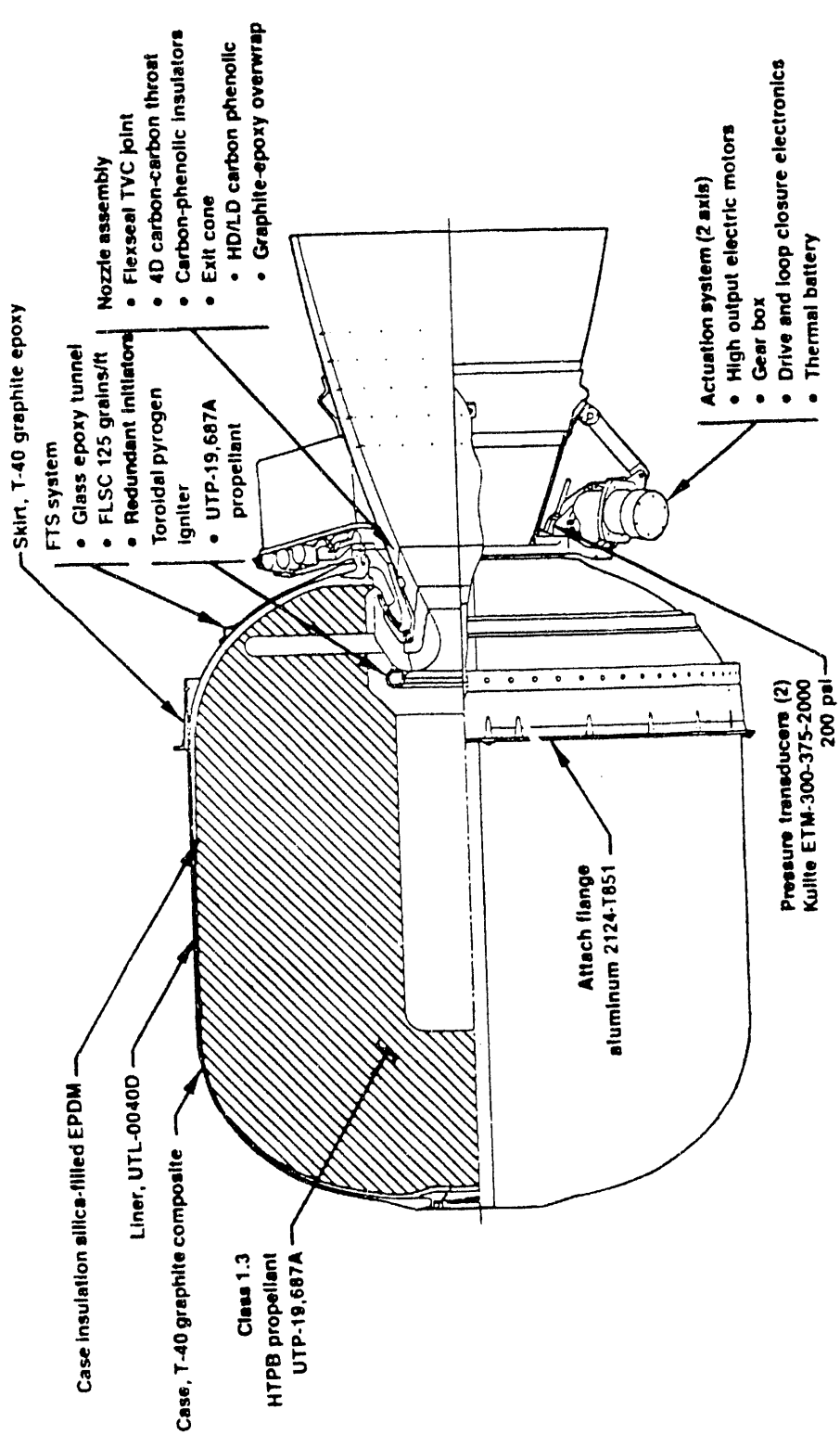

Figure 4: The Orbus 1 STARS Third Stage Motor

A trajectory simulation is used that repeatedly simulates each failure mode. Specific parameters are varied either systematically or randomly (in a Monte Carlo sense) in order to build up a data base correlating failures to debris impact locations. The parameters varied systematically include:

1. the time of failure, varied from 18 to 38 seconds after third stage ignition in one second increments,
2. the failure mode category (four were defined: see page 12),
3. delay time between failure and FTS activation,[1]
4. the fragment class, of which 19 were defined (see Table 2 on page 11).

Parameters varied randomly about nominal, via a statistical model, include

1. the third stage state vector at the time of a component failure,
2. details of the failure mode (such as angle of nozzle position: see page 17),
3. fragment velocities induced by FTS activation,
4. wind profile.

A total of 240 996 different impact points were generated using the various combinations of these parameters for each delay time.[2] In addition, 19 019 trajectory variations of normal mission completion were computed.[3] For each of the systematically varied parameters, a normal (Gaussian) ground impact probability density function (PDF) was defined as a function of latitude and longitude. Each such PDF represents the likelihood that a given fragment of this class will impact in a given unit area on the earth's surface, assuming that the vehicle failed at the assumed time in the assumed mode with the assumed delay prior to FTS activation. For a given spot on the earth, these PDFs are then integrated numerically over all failure times and multiplied by the probability of that failure mode occurring and by the number of fragments in that fragment class. The result is summed with similar results for the other failure modes and fragment classes to obtain the overall probability of any fragment impacting at that spot (per unit area) for the assumed FTS delay interval.

By computing such probabilities over a grid of locations on the earth's surface, an impact probability contour map can be generated. Alternately, a numerical integration over a region of interest can be performed to determine the probability of an impact in that region. From the results of such a calculation, in conjunction with population data, the expected casualty rate can be derived.

---

1. Delay times of 3 and 4 seconds were used, as suggested in discussions with LaPoint and Valencia of the KMR range safety office.
2. 151 state vectors at each of 21 failure times for 4 failure modes and 19 fragment classes.
3. 19 fragment classes for 1001 normal mission completion state vectors at third stage burn out.

Required Assumptions

Due to the number of possible failure scenarios and the complexity of the STARS system, a number of assumptions have been made in order to complete this analysis in a timely manner. Except as noted, each assumption is conservative in nature; i.e., by making the assumption the resulting hazard estimate is greater than that resulting from the implementation of a more accurate model. In this way the estimates of casualty and impact into undesirable areas are assured to be greater than the actual value. Assumptions that might be considered non-conservative are few, and the rational for making these assumptions is given.

The IIP for the STARS M1 mission is several hundred nautical miles away from the Marshall Islands area until after third stage ignition. Therefore, only those vehicle systems which remain during the third stage burn have been considered for the KMR area flight safety. Descriptions of these components, along with reliability estimates, are available in the STARS Flight Safety Data Package and other documents.[4,5]

In addition, the IIP for all off-nominal flights does not come within 100 nm of the nearest inhabited atoll until 20 seconds after third stage ignition. Hence it is assumed that failures prior to 18 seconds after third stage ignition (to be conservative) are not contributors to the hazards in the Marshall Islands area.

The nominal trajectory for these studies was that which was current at the time the work was initiated in the Spring of 1991. Since then, the third stage performance model,[6] the vehicle mass properties,[7] and the estimates of the initial phases of the trajectory have been revised slightly, resulting in a slightly different final nominal trajectory.[8] However, the difference between the nominal trajectory used for this report and the final M1 trajectory is small (less than one standard deviation), since the target points and dogleg turns have not changed and changes to the vehicle physical model is slight. Hence, the preliminary nominal trajectory used for this analysis can be considered fully adequate for the purposes of this report.

---

4. Abbott, K. C. and Plowman, R. W. (7222), *Strategic Target System (STARS) Predicted Mission Reliability for Flight Test Unit - 1 (FTU-1)*, Sandia National Laboratories memo to R. L. Eno (7520) dated October 1, 1990.
5. Abbott, K. C. and Plowman, R. W. (7222), *STARS Third Stage Thrust Vector Actuator (TVA) Assembly Failure Probabilities*, Sandia National Laboratories memo to R. L. Eno (7520) dated September 18, 1990.
6. Outka, David E., *Orbus Flight Motor Performance Data*, Sandia National Laboratories memo to Distribution, dated April 2, 1991.
7. Weber, M. R., *STARS M1 Missile Unclassified Mass Properties*, Sandia National Laboratories memo to Distribution, dated July 30, 1991.
8. Millard, William A., Outka, David E., and White, John E., **Trajectory and Flight Safety for the STARS M1 Mission**, Sandia National Laboratories report to Distribution, dated April 26, 1993.

Fragment Classes

A number of debris fragments are created upon activation of the FTS during third stage burn, and additional fragments are created due to aerodynamic heating and loading. The exact number of such fragments is impossible to predict. To be conservative, a large number of potentially hazardous fragments has been assumed. Specifically, fragments assumed to reach the earth include 106 from payload Test Object 1 (T. O. 1), 24 from payload T. O. 2, and 16 from the third stage. The debris are grouped into fragment classes, as described later, designed to represent the broad range of fragments which might be expected. Note that it is likely that some fragments assumed to reach the earth will actually fully demise due to aerothermal heating. Moreover, some of the fragments counted as hazardous are likely to impact the earth with insufficient energy to pose a safety threat.[9] However, this conservative analysis assumes that all fragments survive aerothermal heating and low energy fragments are not ignored.

Item Number	Fragment Description	Number of Pieces	Mean Incremental Velocity (ft/sec) for Flight Termination Times of				Standard Deviation of Velocity
			2 sec	22 sec	31 sec	38 sec	
1	Thrust Vector Actuator	2	20	74	78	53	15%
2	TVC Electronics Package	1	20	74	78	53	15%
3	Motor Aft Dome and Nozzle	1	20	74	78	53	15%
4	Payload	2	8	16	19	17	4 ft/sec
5	Third Stage Booster	1	8	16	19	17	3 ft/sec

Table 1: Fragment Velocities due to FTS Activation During Third Stage Burn

Considerable attention has been given to the relative velocities imparted to the vehicle fragments upon activation of the FTS while the third stage (Orbus) motor is thrusting. Original estimates were too conservative in that they did not take into account the energy dissipated by the section of case structure not cut by the shaped charge. Subsequently, an analysis has been performed which examines the stress in the aft dome case material following FTS activation.[10,11] It turns out that the un-

9. Energy relationships between impacting fragments and hazard classes are discussed, for example, in Document 315-79, *Risk Analysis Techniques*, prepared by the Range Safety Group, Range Commanders Council, March, 1979

10. Gwinn, K. W., *STARS Thrust Termination with Variable Pressure Loading*, Sandia National Laboratories memo to Bob Mata dated July 25, 1991.

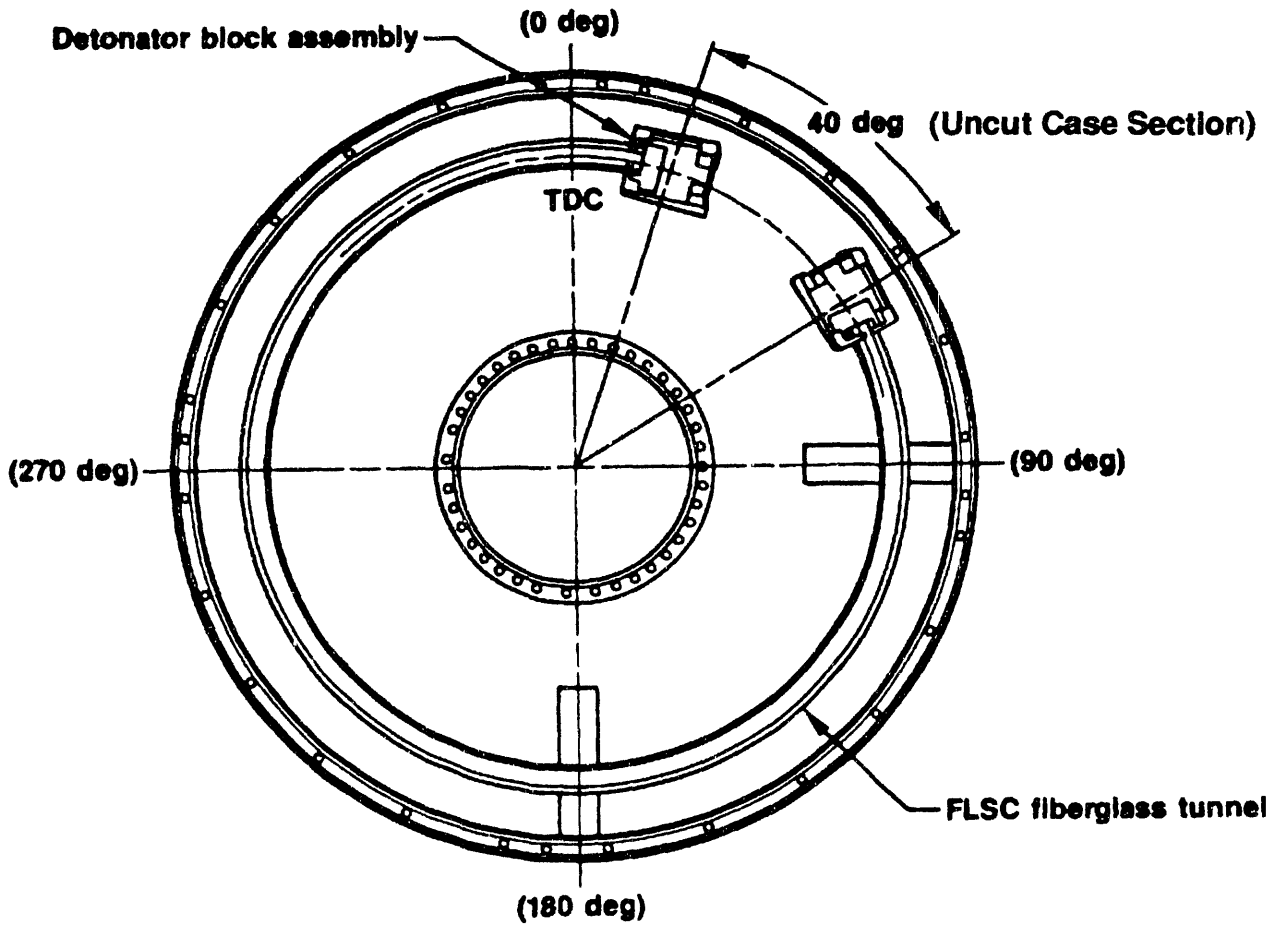

Figure 5: Orbus Motor Aft Dome and Shaped Charge Configuration

cut case section (see Figure 5) absorbs a significant amount of energy. Moreover, the cut portion of the aft dome quickly deforms until it is wrapped around the nozzle and attached TVC components, thus increasing the area available for the hot propellant gas to vent while reducing the area over which the gas can accelerate the aft portions of the motor. The results of this analysis are summarized in Table 1.

To reduce the total required number of trajectory calculations, fragment classes were identified for debris resulting from aerothermal breakup of some of the major fragments. The model for the aerothermal demise of the third stage was developed by Donald L. Potter of Sandia's Thermophysics Department. An overview of the model is sketched in Figure 6. Demise models for the payloads were developed by assuming each undergoes significant breakup and, for T. O. 1, from observation of similar objects tested previously. The 19 fragment classes defined are listed in Table 2.

11. Outka, D. E., *STARS Third Stage Fragment Velocities due to Thrust Termination*, Sandia National Laboratories memo to W. P. Wolfe dated August 7, 1991.

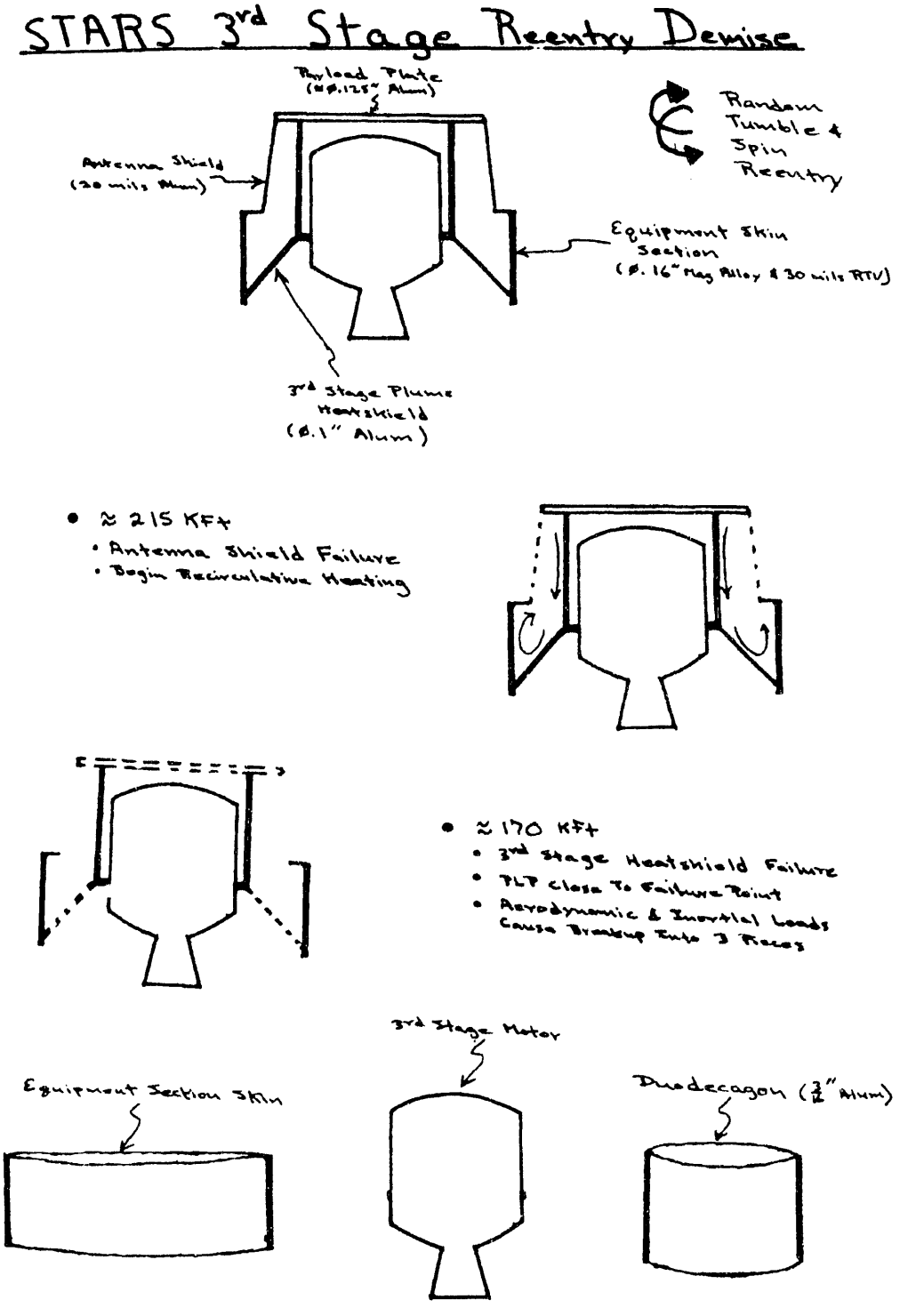

Figure 6: Aerothermal Demise of the STARS Third Stage

Class ID	Description	Quantity	Approximate Mass (lb_m)	Approximate Beta (lb/ft^2)
1	nozzle, aft dome of Orbus motor	1	54.2	50
2	third stage skin (ring)	1	46.9	6 - 13
3	dodecagon with components	10	1.0 - 287	41 - 78
4	spent Orbus motor	1	109.4	10 - 19
5	T. O. 1 mid module	1	44	80 - 500
6	T. O. 1 NTP	1	20 - 30	100 - 800
7	T. O. 1 shell fragment	100	avg: 0.3 max: 1.0	5
8	T. O. 1 structure fragment	1	2	10
9	T. O. 1 structure fragment	2	4	20
10	T. O. 1 structure fragment	1	5	40
11	T. O. 2 module	1	45 - 120	400
12	T. O. 2 module	1	45 - 120	350
13	T. O. 2 module	1	70	70
14	T. O. 2 NTP	1	20 - 30	100 - 800
15	T. O. 2 debris	10	0.1 - 1.0	3
16	T. O. 2 debris	10	0.1 - 1.0	5
17	yaw TVC actuator	1	7	27 - 71
18	pitch TVC actuator	1	7	27 - 71
19	TVC electronics box	1	9.5	16 - 43

Table 2: Fragment Classes Which Impact the Earth's Surface

Third Stage Impact Mode Categories

The term "impact modes" is defined to include failure modes that result in impacts away from the intended target area as well as impacts within the normal target area. The mission flight safety officer (MFSO) will activate the FTS upon recognition that the trajectory has deviated from acceptable flight parameters and can soon endanger protected areas. This analysis assumes two delay times of three and four seconds between failure and FTS activation. The vehicle fragments that result will further disperse due to the relative velocity imparted by the dissipating motor energy, the relative velocity imparted by conversion of the original vehicle's angular velocity into translational velocity, and the varying aerodynamic characteristics of each fragment.

Failure scenarios that occur while the third stage is thrusting and which lead to impacts outside the nominal impact areas can be grouped into several categories:

1. **Tumble Turn Failures.** For an initially stable, exoatmospheric vehicle such as the STARS third stage, a tumble turn occurs when the line of action of the time averaged thrust vector is not aligned with the vehicle's mass center. This will occur when the vehicle autopilot is unable to stabilize the vehicle due to an electronic or mechanical failure. The resulting moment induces an angular acceleration and velocity: the vehicle begins to tumble. The amount to which the IIP deviates from the planned corridor is dependent upon the plane of the tumble (minimum deviation when the tumble plane is vertical, maximum when horizontal), the angular acceleration (the greater the angular acceleration, the sooner the integrated effect of the thrust vector approaches zero), and the time between loss of vehicle control and FTS activation.

   Three tumble turn subcategories have been identified. These deal with specific component failures, the discussion of which begins on page 13.

   1a. The nozzle gimbal angle returns to null (zero deflection, due to zero actuator force).

   1b. The nozzle gimbal angle goes to its physical limits (hard over).

   1c. The nozzle gimbal angle becomes fixed (stuck or frozen nozzle gimbal).

2. **Controlled Turn Failures.** Such a turn occurs when the autopilot is working properly, but the guidance commands to the autopilot are faulty. The result is a turn, potentially at maximum rate and acceleration, toward an incorrect target. It will be shown that the probability of such a chain of events occurring is quite low. If it should occur, the MFSO will activate the FTS upon recognition that the trajectory IIP is approaching protected areas.

3. **Sudden Vehicle Destruction.** The potential exists for the third stage to destruct while still within the normal range of trajectories. This could be due to rupture of the Orbus motor case, to failure of a system unrelated to the vehicle trajectory but upon which the MFSO is dependent for flight safety decisions, or to unintended activation of the FTS by either a system failure or human error. The vehicle fragments that result from such a destruct action will disperse somewhat from the IIP.

4. **Normal Dispersion.** In addition to system failures, the potential exists for a vehicle which operates normally through third stage burn to impact away from the intended point. Causes for such a miss can be related to uncertainty in aerodynamics, winds, motor performance, and navigator errors. Of these, only the latter is likely to be detectable in time for the MFSO to take action. As will be shown, however, none are likely to cause a serious flight safety situation as long as the associated hazard area is accounted for in advance.

Failure Probabilities

The probability that each type of failure might occur can be predicted by examination of the components which lead to the failure.

1. **Tumble Turn Failure Probability.** Failure of any one of a number of components can lead to a tumble turn. The overall probability of such a failure is 5.151×10^{-4}, based on the data given in Table 3. (These data and reference labels were extracted from the Abbott and Plowman report.[4]) For the reliability computation, the time duration (Δt) of interest was taken to be 40 seconds, or 0.4 seconds longer than the nominal burn duration of the third stage Orbus motor. As noted below, the nature of the tumble turn will change depending on which component has failed. A probability for each type of tumble turn has been computed, based on the

Reference Label	Component Description	Failure Rate, Q_J (per 10^6 hours)
J1	Electronics Battery	10 000.0
J2	SANDAC V Battery	10 000.0
J3	Electronics Power Distribution (MA180)	1 037.85
J4	Rate Gyro	200.0
J7	SANDAC V Flight Computer	1 133.869
J11	System Junction (MA173)	239.836
J13	Third Stage TVC	3 390.0
J19	Third Stage TVC / Ignition Battery	10 000.0
J25	ACS Electronics (MA176)	8.207
J38	IMU (Ring Laser) (MA726)	360.4903
Overall Reliability	$\prod_{j \in Q_J} e^{-Q_j \times \Delta t_j} = 0.999485$	

Table 3: Reliability of Components Which Could Cause a Tumble Turn

responsible component reliability data. Some components have more than one failure mode, and so contribute to more than one type of tumble turn. To be conservative, the full failure rate for each such component has been allotted to each tumble turn probability calculation. This approach leads to an overestimation of the likelihood of a tumble turn, but avoids attempting to precisely allocate the probabilities of each distinct mode of failure for each component.

Failure of the items listed in Table 4 can cause loss of signal to the nozzle deflection actuators, causing the nozzle to return to the null (centered) position. For the M-1 mission, the nozzle must be deflected roughly 1° in order to keep the thrust vector passing through the vehicle mass center during third stage burn. A failure which results in the third stage nozzle returning to the null position will produce a strong torque, a correspondingly high angular acceleration, and little deviation of the centroid of the impact points from the nominal IIP. The relative velocities between each fragment induced by both FTS activation and angular velocity prior to fragmentation can, however, cause impacts to disperse.

Reference Label	Component Description	Failure Rate, Q_J (per 10^6 hours)
J1	Electronics Battery	10 000.0
J2	SANDAC V Battery	10 000.0
J3	Electronics Power Distribution (MA180)	1 037.85
J7	SANDAC V	1133.869
J11	System Junction (MA173)	239.836
J19	Third Stage TVC / Ignition Battery	10 000.0
J38	IMU (Ring Laser) (MA726)	360.4903
Overall Reliability = 0.99965011		

Table 4: Component Reliability Potentially Related to a Null-Positioned Nozzle Failure

Similarly, failure of the items listed in Table 5 can cause the actuators to deflect the nozzle hard against its mechanical limits. Again, a fast tumble will be the result.

If the items listed in Table 6 were to fail, the inputs to the TVC electronics would remain fixed at their most recent value. Hence, the nozzle would also remain fixed at that point. For this situation, the nozzle is likely to be positioned such that the thrust vector passes very nearly through the mass center of the vehicle. Hence, tumble rates will build slowly and will still be low at the time of FTS activation.

2. **Controlled Turn Failure Probability.** For a controlled turn to occur, the autopilot software which stabilizes the vehicle (and runs on the SANDAC V flight computer) must be operating properly (otherwise, a tumble turn will result). In order for the autopilot to function properly,

Reference Label	Component Description	Failure Rate, Q_J (per 10^6 hours)
J3	Electronics Power Distribution (MA180)	1 037.85
J4	Rate Gyro	200.0
J7	SANDAC V	1133.869
J11	System Junction (MA173)	239.836
J13	Third Stage TVC	3 390.0
J25	ACS Electronics (MA176)	8.207
J38	IMU (Ring Laser) (MA726)	360.4903
Overall Reliability = 0.99992922		

Table 5: Component Reliability Potentially Related to a Hard-over Nozzle Failure

Reference Label	Component Description	Failure Rate, Q_J (per 10^6 hours)
J7	SANDAC V	1133.869
J11	System Junction (MA173)	239.836
Overall Reliability = 0.99998473		

Table 6: Component Reliability Potentially Related to a Stuck Nozzle Failure

the vehicle angular rates measured by the IMU must be correct (or very nearly so). A controlled turn results from either a grossly incorrect position or velocity being computed by the navigator software, or an incorrect steering command being generated by the guidance software. Both of these functions are resident on a single processor board on the SANDAC, and are successfully tested thousands of times under conditions ranging from nominal to extremely off nominal. A SANDAC hardware failure, due, for example, to radiation, could in theory cause such an error if one or more appropriate memory locations were damaged. A conservative bound on such errors can be computed by assuming all failures of a SANDAC processor board are of the type required to generate a controlled turn. In addition, for this calculation it is assumed that all IMU failures are small enough not to cause instability, yet are sufficient to cause a controlled turn. The failure rate of a SANDAC processor board is 155.470 failures per 10^6 hours and for the IMU is 360.4903 failures per 10^6 hours.[4] Therefore, the combined reliability of these components during the 40 second burn of the third stage motor is given by

$e^{-(\frac{155.470 \times 40}{3600 \times 10^6})} \times e^{-(\frac{360.4903 \times 40}{3600 \times 10^6})} = 0.999994267$, and the likelihood of a controlled turn failure is bounded by 5.733×10^{-6} . Under the conservative assumption that 10 percent of the reachable surface area (for several seconds of IIP propagation from a nominal point) of the earth has been designated as a protected area, the probability of impacting in such an area becomes 5.733×10^{-7} (at most). Since the probability of a controlled turn, obtained using the described conservative assumptions, is significantly smaller than the probability of the other failure modes, controlled turn failures were not addressed further. It will be shown that the more likely failure modes produce very small expected casualty and probability of land impact numbers. The controlled turn numbers are not significant additions.

3. **Sudden Vehicle Destruction Probability.** The Orbus (third stage) motor case failure rate is 360 903 per 10^6 hours, which equates to a failure probability of 4.002×10^{-3} over the 40 second burn duration of the motor.[4] The probability of premature FTS activation has been computed to be 1.0×10^{-7} due to onboard hardware failures.[12] The probabilities of failure of onboard systems which are unrelated to the trajectory but essential to MFSO monitoring of the trajectory are also available. A rigorous estimation of the likelihood of ground based system failure, or of human error causing FTS activation, is beyond the scope of this report. However, a value of 0.01 (1 flight termination in 100 flights) has been assigned. It will be shown (compare Figure 7 with Figure 9) that using a value of even 1.0 changes the expected impact density results only in the immediate region of the nominal IIP trace. This is to be expected since for this scenario the vehicle will be operating correctly up to the point of a ground system related failure. A summary of the component failure rates for sudden vehicle destruct is shown in Table 7.

Reference Label	Component Description	Likelihood of Failure
S3C	Third Stage Motor Case	4.002×10^{-3}
PFTS	Premature FTS Firing due to On-Board Systems	1.0×10^{-7}
BTM	Weak FTS Battery or Loss of TM Signal	1.11×10^{-4}
GSE	Ground System (and related) Error	1.0×10^{-2}
Overall Reliability = 0.9858689		0.0141311

Table 7: Reliability of Components For Which Failure Results in Sudden Vehicle Destruction

12. Blankenau, S. J. (7222), *Reliability Predictions for the STARS Destruct System*, memo to T. L. Downey (7525) dated May 12, 1989.

4. **Normal Dispersion.** Dispersions in the target area following a normal flight have also been considered. Factors which cause these dispersions include motor performance variations, guidance system tolerances, winds, and aerodynamic variations. These factors have been included in the impact density calculations, and, for conservatism, the probability of a normal flight has been assumed to be one. (Note that this is in addition to the probabilities of impact due to failure-mode flights, as discussed above.)

A summary of the probability of each event category that lead to impacts in the downrange area is given in Table 8. A failure probability may be computed from reliability data as simply 1 minus the reliability value.

Failure mode	Probability of Event Occurrence
Nozzle gimbal hard-over (tumble turn)	7.07773×10^{-5}
Nozzle gimbal at null (tumble turn)	3.49884×10^{-4}
Nozzle gimbal stuck (tumble turn)	1.52631×10^{-5}
Controlled turn	5.7328×10^{-6}
Sudden vehicle destruct	0.0141311
Normal flight to target area	1.0
Note that the sum of these probabilities is greater than one, due to the use of conservative assumptions in the derivation of each one	

Table 8: Probability of Events Which Lead to Impacts in the Downrange Area.

Tumble Turn Simulations

For tumble turns, sudden vehicle destruct, and normally concluded flights, estimates of the third stage assembly state vector at various times have been computed using a Monte Carlo approach. This was accomplished using the failure variation preprocessing code MCPRAM[13] (Monte Carlo Preprocessor for AMEER) with the trajectory code AMEER[14] (Aero Mechanical Equation Evaluation Routines) and the fragmentation preprocessing code SAFETIE1[15] (Sandia Analysis of Fragment Trajectories). MCPRAM was developed for fuze effectiveness studies and uses Monte Carlo techniques to produce input files of multiple trajectories for AMEER to solve. MCPRAM allows any standard AMEER input variable to be varied about a designated mean with either a uniform or

13. LaFarge, Robert A., *A Users' Manual for MCPRAM and for the Fuze Options in AMEER*, SAND90-0483, May, 1990.
14. Meyer, Eugene J., *A User's Manual for the AMEER Flight Path Trajectory Simulation Code*, SAND80-2056, December, 1984.
15. LaFarge, Robert A., *Using Monte Carlo Techniques and Parallel Processing for Fragmentation Analysis of Explosive Payloads*, AIAA 92-0653, January, 1992.

normal distribution. MCPRAM also allows for arbitrarily sized groups of correlated parameters to be randomly varied. A covariance matrix is used to model the correlation among the parameters.

For the tumble turn analysis, two approaches were used to generate fragment impact distributions. Both used MCPRAM and AMEER to compute the position and velocity of the third stage after each specified failure mode and after a specified delay time (either 3 or 4 seconds) before activating the FTS. In addition to the tumble turn failure modes, the instantaneous flight termination (zero delay time) and normal flight completion scenarios were also investigated. This information was used by SAFETIE1 as initial conditions for that portion of the analysis that investigates the effects of FTS activation and dispersion due to the atmosphere. The resulting state vectors were used by SAFETIE1 to produce initial conditions to AMEER for computing trajectories to investigate the effects of FTS activation and dispersion due to the atmosphere.

In the first approach used for impact point generation, covariance matrices that model the uncertainties in the third stage nominal position and velocity were included. The covariance matrices were generated from data obtained from a study of the effects on the trajectory of 3 σ variations of certain parameters such as propellent weight, specific impulse, and thrust factor.[16] Additionally, the rocket motor nozzle deflection angles were varied to simulate the three types of failure modes under investigation, i.e., stuck nozzle, return to the null position nozzle, and an arbitrary direction, hard-over nozzle. Each failure mode and each delay time generated a separate impact distribution.

The second approach eliminated the initial-state covariances matrices. The resulting impact distributions can be used to produce impact areas about the nominal trajectory. These ellipses can be superimposed over the current trajectory in a real-time flight safety software system to help the MFSO determine if the FTS should be activated.

Statistical Modeling of the Failure Modes

For each of the tumble turn failure modes, the nozzle deflection angles were either kept constant or were varied with uniform or normal distributions. The variable PHMTRD is the angle which defines the plane of the nozzle deflection in roll, and the variable XIMTRD is the angle of deflection from the longitudinal vehicle axis. To simulate the hard-over nozzle gimbal angle failure mode, XIMTRD was given a constant value of 3.0 degrees (a conservatively small estimate of the physical limitation of the Orbus nozzle), and PHMTRD was given a uniform distribution between 0 and 360 degrees. To simulate the nozzle gimbal return to the null failure mode, XIMTRD was given a normal distribution with a mean of 0 degrees and a standard deviation of 0.27 degrees.[17] PHMTRD was given a uniform distribution between 0 and 180 degrees. In both models, the nominal mass center offsets were included in the analysis. For the stuck nozzle gimbal failure mode, the relevant parameter is the offset of the thrust vector from the center of mass, not the actual noz-

16. Study performed by John White of the Sandia National Laboratories Navigation, Guidance, and Control System Department.

17. This standard deviation estimate is based on changes in the nozzle null orientation due to motor case flexibility under operational pressures.

zle gimbal angle. To simplify the calculations, the mass asymmetries were removed so that the nozzle angle that produces a null thrust moment would not have to be computed at each time of the analysis. XIMTRD was given a normal distribution with a mean of 0 degrees and a standard deviation of 0.02 degrees,[18] and PHMTRD was given a uniform distribution between 0 and 180 degrees. For each failure mode, 151 random trajectories were computed at each one-second increment along the trajectory from 18 seconds to 38 seconds after third stage ignition. For each failure mode, a post-processor was used to extract (from the nominal AMEER output file) the file of 3171 ((38-18+1)x151) state vectors for each specified delay time. These state vectors were used as initial conditions for the SAFETIE1 portion of the analysis. The effects of each of the tumble turn failure modes were investigated for the both with and without initial state variation. A total of fourteen files of 3171 state vectors were produced for this analysis.

Fragment Impact Distribution

For a given tumble turn analysis approach, failure mode, and delay time, SAFETIE1 assumed that the file of 3171 state vectors describes the position, velocity, angular orientation, and angular velocity of the third stage assembly at the time of FTS activation. For each of the seven initial fragment classes[19] a random incremental velocity was computed, based on the statistical models in Table 1. The total velocity vector of each fragment was computed by adding the incremental velocity vector and $\overline{V}_{\omega}$ (the velocity vector caused by the angular velocity of the third stage assembly) to the velocity vector of the third stage assembly before FTS activation. The velocity vector $\overline{V}_{\omega}$ is computed by taking the vector cross product of the third stage angular velocity and the vector describing the difference in location between the third stage cg and the cg of the appropriate fragment. Aerothermal/structural analysis has indicated that the two payloads and the third stage booster would breakup near 150 000 feet altitude. The trajectory simulations included this further fragmentation, resulting in the 19 fragment classes and associated trajectories (shown in Table 2 on page 11) from that altitude down to impact.

A total of 843 486 trajectories were computed.[20] Each fragment was modeled as a point mass in AMEER with an appropriate drag model (tumbling cube, tumbling cylinder, or the payload). The Kwajalein annual statistical wind model was used in all the trajectories.[21] For a given altitude, the wind model uses five statistical parameters. In Cartesian coordinates, these parameters are the means and standard deviations of the two orthogonal wind velocity components and the correlation coefficient between the two components. All 19 fragments from a given FTS action fall through

18. This standard deviation estimate is derived from the time history of the offset of the thrust vector relative to the vehicle mass center when the gimbal is actively controlled.
19. Defined in Table 1:Two thrust vector activators, 1 TVC electronics package, 1 motor aft dome nozzle, 2 payloads, and 1 third stage booster.
20. 843 486 = (19x((2x3)+1)x3171x2): 19 fragment classes, 2 destruct delay times, 3 tumble turn failure modes, 1 sudden destruct failure mode, 3171 time-of-destruct state vectors, with and without pre-failure state vector variations.
21. *Kwajalein Missile Range, Kwajalein, Marshall Islands, Range Reference Atmosphere, 0 - 70 km Altitude*, Document 360-82, published by Range Commanders Council, White Sands Missile Range, New Mexico.

the same wind profile. The impact distributions for the initial state vector covariance approach are shown in Figures 1-7, and the impact distributions which result from failures off the nominal trajectory are shown in Figures 8-14.

Computation of the Impact Density Map

The impact data generated using Monte Carlo techniques can be used to develop a statistical model of the impact likelihood on the earth's surface. The statistical model is built up from subsets of the impact data, where each subset consists of all the impacts resulting from a given combination of the systematically varied impact mode parameters. For impacts resulting from failures, the systematically varied impact mode parameters are the failure time, the fragment class, the failure type, and the delay time between the failure and FTS activation. One hundred fifty-one (151) impacts were generated for each subset by the Monte Carlo technique described previously. For normally completed flights, only the fragment class is systematically varied. One thousand one (1001) impacts were generated for each subset of normally completed flights.

For the discussion which follows, analysis of impacts from normally completed flights is a subset of the analysis applied to failure mode impacts. When the differences are not obvious, they will be noted explicitly.

The impact points vary due to the random variations in failure-time state vector, the nozzle position (see page 18), the fragment velocities (induced by both FTS activation and the angular velocity which results from a tumble turn), and the wind profile. Since two or more of these variations are Gaussian in nature, it can be expected that for each such subset the impact point variations will also approximate a Gaussian distribution. Hence, for each such subset, five parameters describing the corresponding Gaussian impact point distribution function are computed: mean longitude and latitude, standard deviations in longitude and latitude, and the correlation coefficient relating deviations from the mean in longitude with those in latitude. This function describes the impact probability density function (PDF) given that the prescribed conditions[22] are valid.

The equations for the defining parameters for the functions are given in Table 9. λ_i is the i^{th} impact longitude of the subset, δ_i is the i^{th} impact latitude of the subset, and n is the number of impact points in the subset. The value of the PDF function at an arbitrary longitude, λ, and latitude, δ, is given by the bivariate Gaussian density function, as shown in Table 10. Note that it is an exponential function of the five defining parameters given in Table 9. To obtain the impact density function for all combinations of the time of failure, fragment class, and type of failure, the subset PDFs are combined numerically in the following manner.

First, a grid of latitude-longitude points in the area of interest is defined. The number of impacts per unit area is computed at each of the grid points. For each grid point and combination of impact mode and fragment class, the density of impacts expected for all times of the impact mode is ob-

22. Failure time, fragment class, failure type, and delay time between failure and FTS activation

mean longitude	$\bar{\lambda} = \frac{1}{n}\sum_{i=1}^{n}\lambda_i$
mean latitude	$\bar{\delta} = \frac{1}{n}\sum_{i=1}^{n}\delta_i$
standard deviation of longitude	$\sigma_\lambda = \sqrt{\frac{1}{n-1}\sum_{i=1}^{n}(\lambda_i-\bar{\lambda})^2}$
standard deviation of latitude	$\sigma_\delta = \sqrt{\frac{1}{n-1}\sum_{i=1}^{n}(\delta_i-\bar{\delta})^2}$
correlation coefficient	$\rho_{\lambda\delta} = \frac{\sum_{i=1}^{n}[(\lambda_i-\bar{\lambda})(\delta_i-\bar{\delta})]}{\sqrt{\sum_{i=1}^{n}(\lambda_i-\bar{\lambda})^2}\sqrt{\sum_{i=1}^{n}(\delta_i-\bar{\delta})^2}}$

Table 9: The Defining Parameters for the Impact Probability Density Functions

$$pdf(\lambda,\delta) = \frac{e^{\left\{\frac{-1}{2(1-\rho_{\lambda\delta}^2)}\left[\frac{(\lambda-\bar{\lambda})^2}{\sigma_\lambda^2} - \frac{2\rho_{\lambda\delta}(\lambda-\bar{\lambda})(\delta-\bar{\delta})}{\sigma_\lambda\sigma_\delta} + \frac{(\delta-\bar{\delta})^2}{\sigma_\delta^2}\right]\right\}}}{2\pi\sigma_\lambda\sigma_\delta\sqrt{1-\rho_{\lambda\delta}^2}}$$

Table 10: The Bivariate Gaussian Density Function for the Impact Probability Density Functions

tained. This is done for failure impact modes by numerically integrating in time the value of the PDFs obtained for each subset described above at the grid point, and multiplying the integrand with the likelihood of the failure occurring over the time interval of integration and by the number of pieces in the given fragment class. For the normal mission completion impact mode, integration over time is not necessary since no time variation is relevant. Instead, the subset PDF is evaluated at the grid point and multiplied by the likelihood of normal mission completion and by the number of pieces in the given fragment class. The result is summed with similar results for all other combinations of impact mode and fragment class. This sum is the number of impacts per unit area which can be expected at the grid point from all impact modes.

$$id(\lambda,\delta) = \sum_{j \in \text{f.c.}} N_j \left[P_{\text{n.c.}} pdf_j(\lambda,\delta) + \sum_{i \in \text{f.m.}} \left[\int_{18}^{38} (P_i)\, pdf_{i,j}(\lambda,\delta)\, dt \right] \right]$$

Where:	id()	impact density function
	λ	longitude
	δ	latitude
	f.c.	fragment class
	N	number of fragments in the fragment class
	P	probability
	n.c.	normal completion
	f.m.	failure mode
	pdf()	probability density function
	t	time since third stage ignition

Table 11: The Impact Density Function for an Arbitrary Longitude and Latitude

This process is repeated for every point in the grid for each delay time of interest. The results are plotted as a contour plot with independent axes of longitude and latitude. These contours are plotted in Figure 7 for the 3 second FTS delay and Figure 8 for the 4 second FTS delay.

To demonstrate that the (unknown) likelihood of FTS activation by ground system error does not greatly affect the contour lines less than 10^{-6}, the data has been recalculated with the spontaneous destruct probability of 1.0. (This is in contrast to the value of 0.0141311 used for all other calculations, and discussed on page 16). The corresponding plots are given in Figure 9 and Figure 10.

A similar technique is used to compute the probability of land impact, the expected casualty (E_c) value for each island (Tables 12 and 13), and the probability of an impact in the various keep-out zones (Table 14). The Gaussian impact distribution functions used to compute the data for the contour plots are used to compute the number of impacts per unit area expected at points within populated land areas and keepout zones. The expected casualty values assume all fragments are hazardous, that each person occupies a distinct 32 square feet area, and that an impact within such an area causes a casualty. Land impact calculations multiply the number of impacts per unit area by the land area of interest. The expected number of impacts within a keepout zone is computed by integrating the point values of the number of impacts per unit area over the area of the keepout zones.

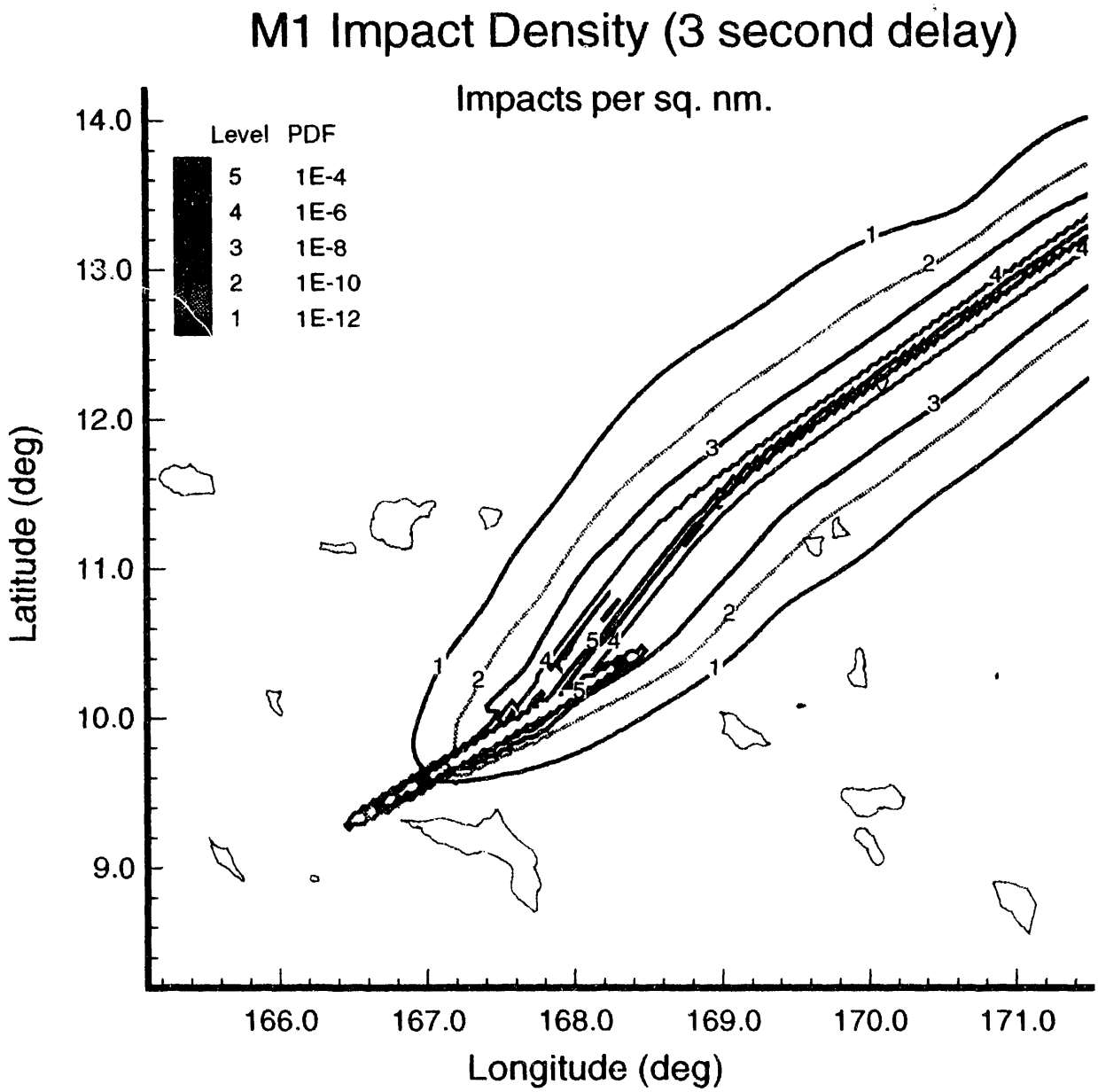

Figure 7: Impact Density Map: 3 Second Delay Between Failure and FTS Activation

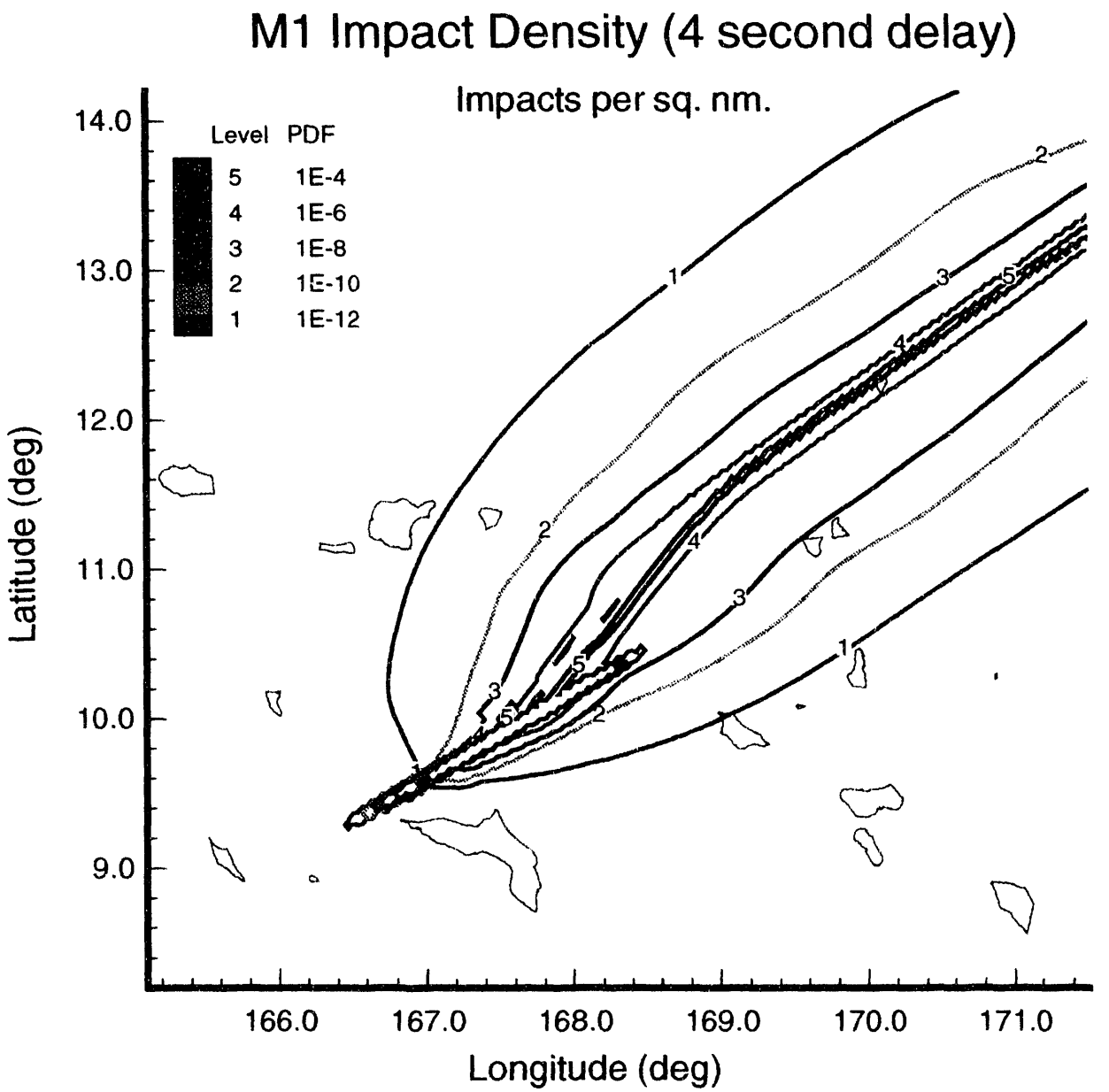

Figure 8: Impact Density Map: 4 Second Delay Between Failure and FTS Activation

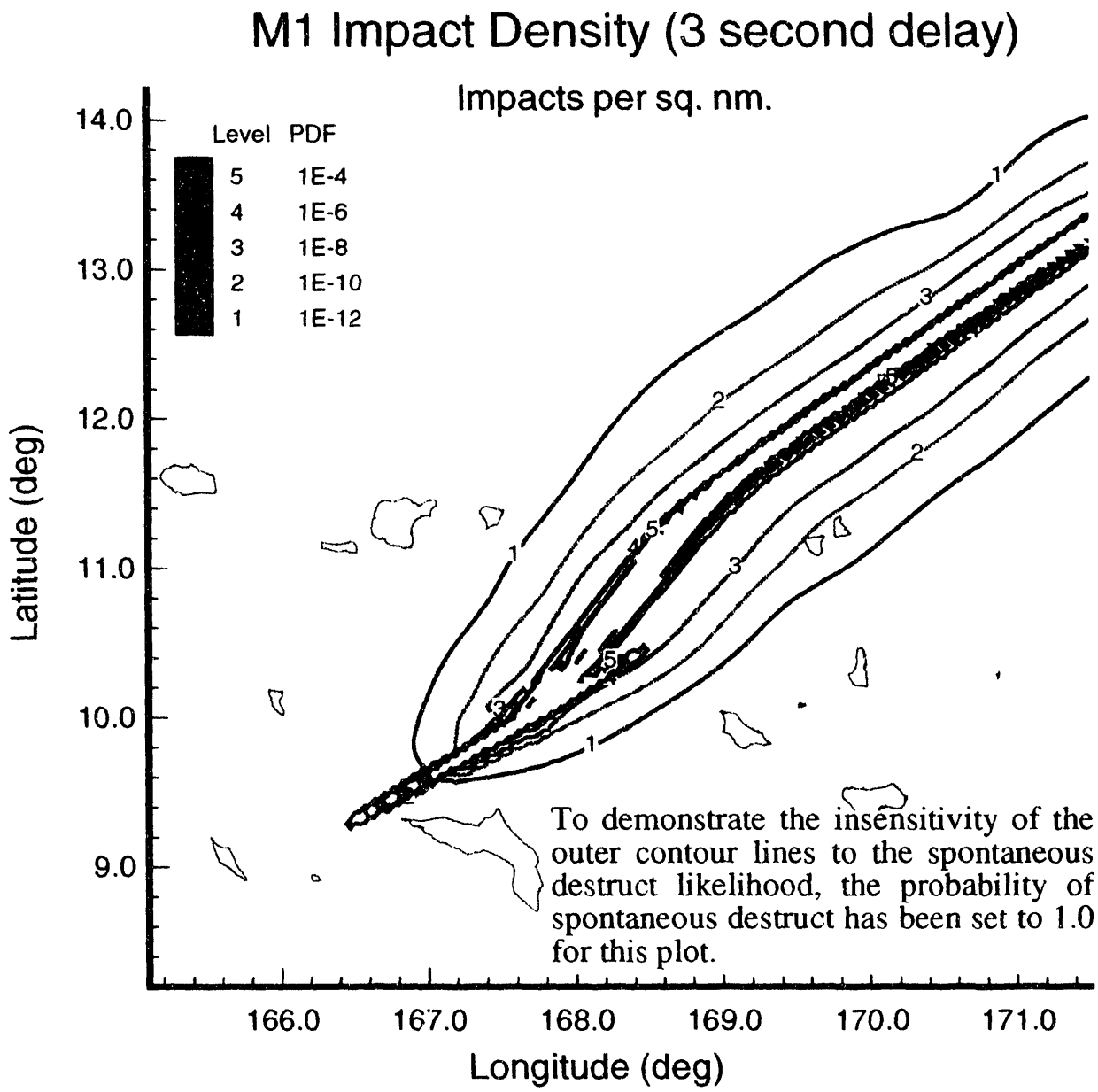

Figure 9: Impact Density Map: 3 Second Delay Between Failure and FTS Activation,
Spontaneous Destruct Probability = 1.0

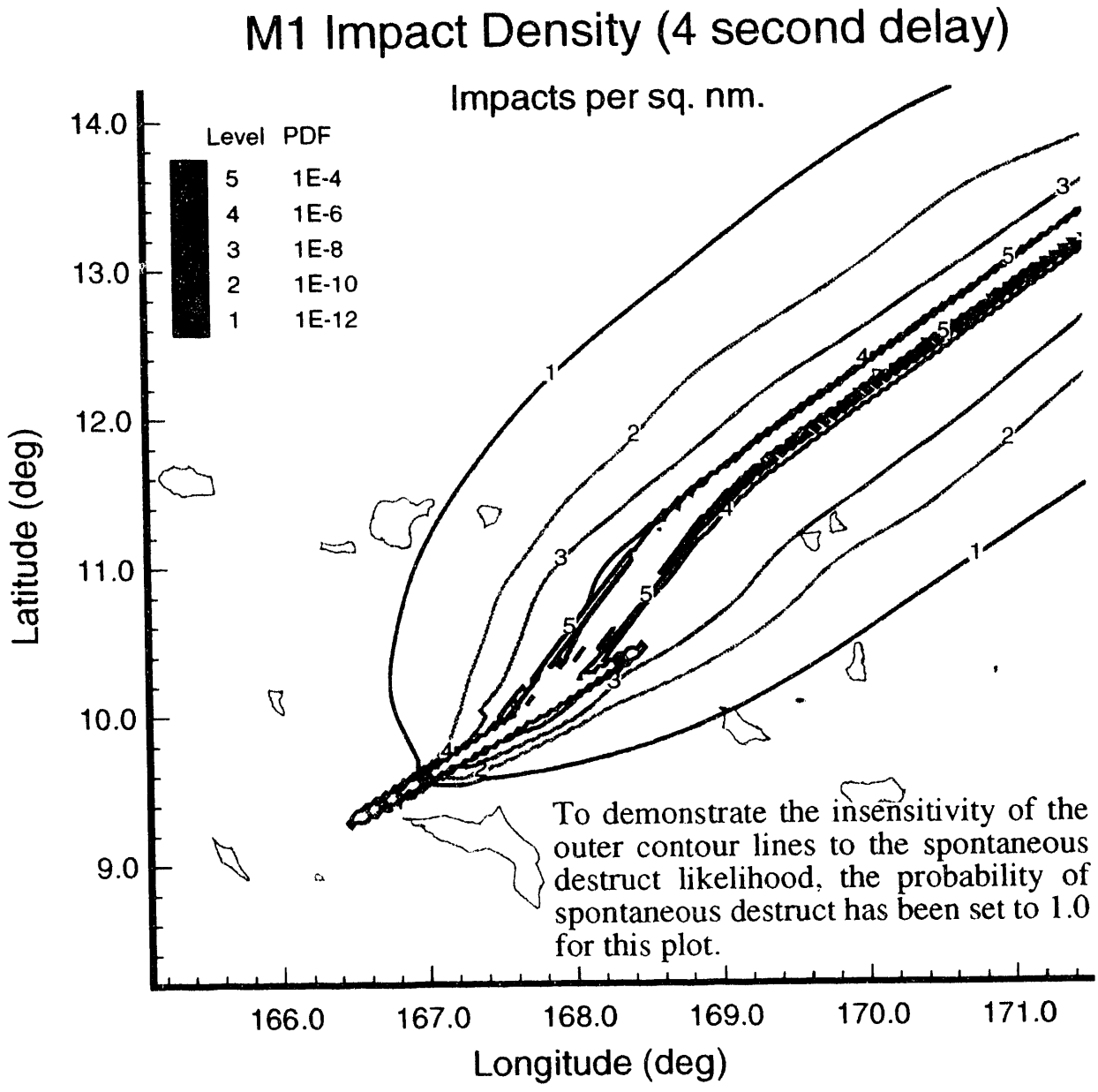

Figure 10: Impact Density Map: 4 Second Delay Between Failure and FTS Activation,
Spontaneous Destruct Probability = 1.0

Table 12: Land Impact Probabilities and Expected Casualties: 3 Second FTS Delay

Name	Land Area sq. nm.	N. Lat deg.	E. Long deg.	Population	Land Impact Probability	Expected Casualties
Ailinginae Atoll						
Majokoryaan	0.118	11.1320	166.5270	0	2.92074×10^{-22}	0
Bikar Atoll						
Bikar	0.065	12.1862	170.1033	0	8.57815×10^{-08}	0
Bikini Atoll						
Bikini	0.632	11.6277	165.5458	0	1.73412×10^{-35}	0
Ailuk Atoll						
Ailuk	0.204	10.217	169.982	465	6.91392×10^{-20}	1.36598×10^{-22}
Enijabro	0.145	10.4504	169.9563	3	7.42574×10^{-18}	1.33165×10^{-22}
Kapen	0.223	10.4588	169.9500	4	1.42945×10^{-17}	2.2224×10^{-22}
Erikub Atoll						
Erikub	0.136	9.0200	170.0616	0	1.47325×10^{-35}	0
Kwajalein Atoll						
Big Bustard	0.009	8.762	167.739	7	5.14455×10^{-29}	3.46817×10^{-32}
Biggerann	0.152	9.337	167.060	12	7.35192×10^{-17}	5.03079×10^{-21}
Ebadon	0.350	9.328	166.827	38	5.40554×10^{-17}	5.08689×10^{-21}
Ebeye	0.088	8.780	167.739	8500	1.18378×10^{-27}	9.91072×10^{-29}
Ebioaji	0.023	8.836	167.740	10	4.22309×10^{-27}	1.59148×10^{-30}
Eniwetak	0.018	9.017	167.716	4	1.23805×10^{-23}	2.38464×10^{-27}
Ennubirr	0.038	9.366	167.496	380	2.97965×10^{-17}	2.58264×10^{-19}
Ennylabegan	0.155	8.799	167.618	98	1.97824×10^{-26}	1.0841×10^{-29}
Enubuj	0.105	8.749	167.685	60	6.0313×10^{-28}	2.98724×10^{-31}
Gagan	0.009	9.288	167.538	8	5.14867×10^{-19}	3.9668×10^{-22}
Gellinam	0.009	9.099	167.729	6	1.47324×10^{-22}	8.51295×10^{-26}

Table 12: Land Impact Probabilities and Expected Casualties: 3 Second FTS Delay

Name	Land Area	N. Lat	E. Long	Population	Land Impact Probability	Expected Casualties
	sq. nm.	deg.	deg.			
Gugeegue	0.073	8.849	167.744	10	2.33017×10^{-26}	2.7667×10^{-30}
Kwajalein	0.948	8.723	167.737	3446	8.55125×10^{-28}	2.69423×10^{-30}
Legan	0.035	8.984	167.579	6	2.2085×10^{-23}	3.28155×10^{-27}
Little Bustard	0.003	8.755	167.737	5	1.25703×10^{-29}	1.81591×10^{-32}
Meck	0.047	9.003	167.727	255	1.60705×10^{-23}	7.55735×10^{-26}
Omelek	0.012	9.050	167.743	1	2.40882×10^{-23}	1.73989×10^{-27}
Roi-Namur	0.510	9.396	167.476	470	1.04913×10^{-15}	8.38023×10^{-19}
Lae Atoll						
Lae	0.230	8.921	166.264	192	1.78428×10^{-24}	1.29102×10^{-27}
Lib Island	0.230	8.3160	167.3800	140	8.19832×10^{-36}	4.32537×10^{-39}
Likiep Atoll						
Jibal	0.156	9.888	169.276	70	8.61484×10^{-19}	3.35057×10^{-22}
Lado	0.189	9.8425	169.3105	20	2.22582×10^{-19}	2.04154×10^{-23}
Likeip	0.510	9.823	169.303	406	4.19976×10^{-19}	2.89786×10^{-22}
Mato	0.461	10.044	168.997	30	2.1596×10^{-15}	1.21812×10^{-19}
Mero	0.148	9.895	169.265	60	1.11568×10^{-18}	3.92037×10^{-22}
Maleolap Atoll						
Airik	0.204	8.5033	171.1980	220	7.85052×10^{-55}	7.33819×10^{-58}
Kaven	0.612	8.8983	170.8460	95	2.96082×10^{-43}	3.98367×10^{-47}
Ollot	0.102	8.7708	171.1810	80	8.09349×10^{-50}	5.50204×10^{-53}
Tar	0.081	8.8383	171.0967	29	9.1814×10^{-48}	2.84918×10^{-51}
Tjan	0.102	8.9075	170.8950	0	2.35394×10^{-44}	0
Mejit Island	0.642	10.284	170.870	320	1.8464×10^{-24}	7.97697×10^{-28}
Rongelap	0.788	11.157	166.871	165	3.22866×10^{-18}	5.85974×10^{-22}

Table 12: Land Impact Probabilities and Expected Casualties: 3 Second FTS Delay

Name	Land Area	N. Lat	E. Long	Population	Land Impact Probability	Expected Casualties
	sq. nm.	deg.	deg.			
Ujae	0.394	8.930	165.761	209	3.14854×10^{-27}	1.44763×10^{-30}
Utirik	1.283	11.226	169.852	256	1.25379×10^{-11}	2.16839×10^{-15}
Wotho	0.875	10.169	166.011	89	3.50904×10^{-23}	3.09363×10^{-27}
Wotje Atoll						
Ormed	0.254	9.554	170.151	210	3.61271×10^{-28}	2.58891×10^{-31}
Wotje	0.718	9.457	170.241	252	1.36471×10^{-29}	4.1516×10^{-33}

Table 13: Land Impact Probabilities and Expected Casualties: 4 Second FTS Delay

Name	Land Area	N. Lat	E. Long	Population	Land Impact Probability	Expected Casualties
	sq. nm.	deg.	deg.			
Ailinginae Atoll						
Majokoryaan	0.118	11.1320	166.5270	0	4.64495×10^{-15}	0
Bikar Atoll						
Bikar	0.065	12.1862	170.1033	0	1.24507×10^{-07}	0
Bikini Atoll						
Bikini	0.632	11.6277	165.5458	0	2.48726×10^{-19}	0
Ailuk Atoll						
Ailuk	0.204	10.217	169.982	465	9.39821×10^{-15}	1.8568×10^{-17}
Enijabro	0.145	10.4504	169.9563	3	7.13436×10^{-14}	1.2794×10^{-18}
Kapen	0.223	10.4588	169.9500	4	1.22214×10^{-13}	1.90009×10^{-18}
Erikub Atoll						
Erikub	0.136	9.0200	170.0616	0	1.15955×10^{-21}	0
Kwajalein Atoll						
Big Bustard	0.009	8.762	167.739	7	1.09904×10^{-20}	7.40914×10^{-24}
Biggerann	0.152	9.337	167.060	12	1.4435×10^{-15}	9.87765×10^{-20}
Ebadon	0.350	9.328	166.827	38	1.54692×10^{-15}	1.45573×10^{-19}
Ebeye	0.088	8.780	167.739	8500	1.45166×10^{-19}	1.21535×10^{-20}
Ebioaji	0.023	8.836	167.740	10	9.6809×10^{-20}	3.64826×10^{-23}
Eniwetak	0.018	9.017	167.716	4	1.58222×10^{-18}	3.04755×10^{-22}
Ennubirr	0.038	9.366	167.496	380	8.24113×10^{-16}	7.14307×10^{-18}
Ennylabegan	0.155	8.799	167.618	98	4.12272×10^{-19}	2.25931×10^{-22}
Enubuj	0.105	8.749	167.685	60	1.1132×10^{-19}	5.51358×10^{-23}
Gagan	0.009	9.288	167.538	8	6.03562×10^{-17}	4.65016×10^{-20}
Gellinam	0.009	9.099	167.729	6	2.90493×10^{-18}	1.67858×10^{-21}
Gugeegue	0.073	8.849	167.744	10	3.79718×10^{-19}	4.50854×10^{-23}

Table 13: Land Impact Probabilities and Expected Casualties: 4 Second FTS Delay

Name	Land Area	N. Lat	E. Long	Population	Land Impact Probability	Expected Casualties
	sq. nm.	deg.	deg.			
Kwajalein	0.948	8.723	167.737	3446	6.06719×10^{-19}	1.91158×10^{-21}
Legan	0.035	8.984	167.579	6	2.08464×10^{-18}	3.0975×10^{-22}
Little Bustard	0.003	8.755	167.737	5	3.26939×10^{-21}	4.72295×10^{-24}
Meck	0.047	9.003	167.727	255	3.23794×10^{-18}	1.52268×10^{-20}
Omelek	0.012	9.050	167.743	1	1.73415×10^{-18}	1.25257×10^{-22}
Roi-Namur	0.510	9.396	167.476	470	1.75154×10^{-14}	1.39909×10^{-17}
Lae Atoll						
Lae	0.230	8.921	166.264	192	4.45395×10^{-19}	3.22267×10^{-22}
Lib Island	0.230	8.3160	167.3800	140	2.75686×10^{-22}	1.4545×10^{-25}
Likiep Atoll						
Jibal	0.156	9.888	169.276	70	1.02418×10^{-14}	3.98335×10^{-18}
Lado	0.189	9.8425	169.3105	20	5.93128×10^{-15}	5.4402×10^{-19}
Likeip	0.510	9.823	169.303	406	1.31156×10^{-14}	9.04988×10^{-18}
Mato	0.461	10.044	168.997	30	7.4375×10^{-13}	4.19513×10^{-17}
Mero	0.148	9.895	169.265	60	1.12102×10^{-14}	3.93913×10^{-18}
Maleolap Atoll						
Airik	0.204	8.5033	171.1980	220	2.98603×10^{-29}	2.79116×10^{-32}
Kaven	0.612	8.8983	170.8460	95	2.24421×10^{-24}	3.01948×10^{-28}
Ollot	0.102	8.7708	171.1810	80	2.17078×10^{-27}	1.47572×10^{-30}
Tar	0.081	8.8383	171.0967	29	1.19615×10^{-26}	3.71189×10^{-30}
Tjan	0.102	8.9075	170.8950	0	2.85303×10^{-25}	0
Mejit Island	0.642	10.284	170.870	320	2.55216×10^{-16}	1.10261×10^{-19}
Rongelap	0.788	11.157	166.871	165	3.40495×10^{-13}	6.17968×10^{-17}
Ujae	0.394	8.930	165.761	209	7.59224×10^{-20}	3.49075×10^{-23}

Table 13: Land Impact Probabilities and Expected Casualties: 4 Second FTS Delay

Name	Land Area	N. Lat	E. Long	Population	Land Impact Probability	Expected Casualties
	sq. nm.	deg.	deg.			
Utirik	1.283	11.226	169.852	256	1.19955×10^{-09}	2.07457×10^{-13}
Wotho	0.875	10.169	166.011	89	2.89305×10^{-15}	2.55057×10^{-19}
Wotje Atoll						
Ormed	0.254	9.554	170.151	210	1.84487×10^{-18}	1.32205×10^{-21}
Wotje	0.718	9.457	170.241	252	8.46544×10^{-19}	2.57527×10^{-22}

Table 14: Probabilities of Impacts Within Keepout Zones

Names of Reference Areas	Keep-out Circle radius	Center Longitude	Center Latitude	Expected Number of Impacts	
	nm.	deg.	deg.	FTS Delay 3 Seconds	FTS Delay 4 Seconds
Ailinglapalap Atoll	24.00	168.700	7.380	0.	0.362131×10^{-24}
Ailuk Atoll	21.00	169.950	10.330	0.199252×10^{-12}	0.719298×10^{-09}
Aron Atoll	21.00	171.660	7.150	0.	0.118654×10^{-37}
Aur Atoll	16.80	171.169	8.220	0.	0.891691×10^{-26}
Bikini Atoll	27.00	165.400	11.600	0.404341×10^{-29}	0.175950×10^{-14}
Ebon Atoll	15.00	168.690	4.610	0.	0.
Enewetak Atoll	24.00	162.384	11.425	0.	0.712605×10^{-33}
Jabwot Island	12.60	168.980	7.756	0.	0.433553×10^{-23}
Jaluit Atoll	21.60	169.600	6.000	0.	0.707375×10^{-41}
Kili Island	13.20	169.118	5.646	0.	0.
Kwajalein Atoll NE (Roi Namur, Gagan, Ennubirr)	15.60	167.500	9.300	0.237118×10^{-11}	0.218998×10^{-10}
Kwajalein Atoll East Middle (Eniwetak, Gellinam, Meck, Omelek)	15.00	167.730	9.050	0.172174×10^{-15}	0.367121×10^{-12}
Kwajalein Atoll SE (Kwajalein, etc)	16.20	167.680	8.800	0.290050×10^{-19}	0.989938×10^{-14}
Kwajalein Atoll South Middle (Legan)	12.60	167.579	8.984	0.139245×10^{-16}	0.782281×10^{-13}
Kwajalein Atoll NW (Ebadon)	12.00	166.827	9.328	0.288655×10^{-06}	0.288655×10^{-06}
Kwajalein Atoll NW (Biggerann)	12.60	167.060	9.337	0.288059×10^{-11}	0.113963×10^{-10}
Lae Atoll	12.60	166.262	8.921	0.386452×10^{-19}	0.220065×10^{-14}

Table 14: Probabilities of Impacts Within Keepout Zones

Names of Reference Areas	Keep-out Circle radius	Center Longitude	Center Latitude	Expected Number of Impacts	
	nm.	deg.	deg.	FTS Delay 3 Seconds	FTS Delay 4 Seconds
Lib Island	12.60	167.378	8.313	0.344117×10^{-29}	0.147348×10^{-17}
Likiep Atoll	22.80	169.100	9.900	0.675902×10^{-11}	0.154106×10^{-08}
Majuro Atoll	21.60	171.250	7.100	0.	0.596141×10^{-36}
Maloelap Atoll	24.00	171.000	8.750	0.153736×10^{-38}	0.382122×10^{-20}
Megit Island	12.60	170.870	10.284	0.170353×10^{-19}	0.375849×10^{-12}
Mili Atoll	22.80	171.825	6.125	0.	0.
Namorik Atoll	13.20	168.127	5.613	0.	0.168156×10^{-42}
Namu Atoll	22.80	168.140	8.000	0.715125×10^{-36}	0.725901×10^{-19}
Rongelap Atoll	0.60	166.871	11.357	0.622345×10^{-18}	0.225715×10^{-12}
Ujae Atoll	24.00	165.650	9.050	0.943908×10^{-21}	0.411400×10^{-14}
Ujelang Atoll	21.60	160.949	9.776	0	0.951664×10^{-40}
Utirik Atoll	18.00	169.800	11.276	0.191749×10^{-06}	0.956075×10^{-05}
Wotho Atoll	18.00	166.011	10.119	0.512677×10^{-17}	0.561369×10^{-11}
Wotje Atoll	27.00	170.000	9.400	0.598931×10^{-21}	0.735401×10^{-13}

Conclusions

The expected casualty value (E_c, the likelihood that the STARS M1 flight will cause a casualty) in the Marshall Islands area is no greater than 2.08×10^{-13}, which compares favorably to the generally accepted[1] value of 10^{-6}. The probability of a debris fragment impacting an inhabited land area is less than 1.20×10^{-9}. The probability of a debris fragment impacting within the keep-out zones (as defined in Table 14) is less than 1.92×10^{-7} or 9.56×10^{-6} for 3 or 4 second flight termination system delays, respectively.

Presentations of these results to the ranges has been received favorably. Moreover, an analysis done by Tybrin Corp. under contract by KMR has apparently resulted in similar numbers (although Sandia has not received a copy of their final report.) Hence, it is anticipated that the ranges will not deny range safety approval for STARS M1 based on the downrange portion of the flight (which is the subject of this report).

1. Keese, David L., and Barton, William R., *Risk Assessment and Its Application to Flight Safety Analysis*, SAND89-1982.

Appendix A. Raw Impact Data Plots

Appendix A contains plots which show the results of the investigation of the tumble turn failure modes. The plots show the fragment impact distributions for the hard-over nozzle, stuck nozzle, and return to null position failure modes as well as the results of investigation of the instantaneous destruct failure mode.

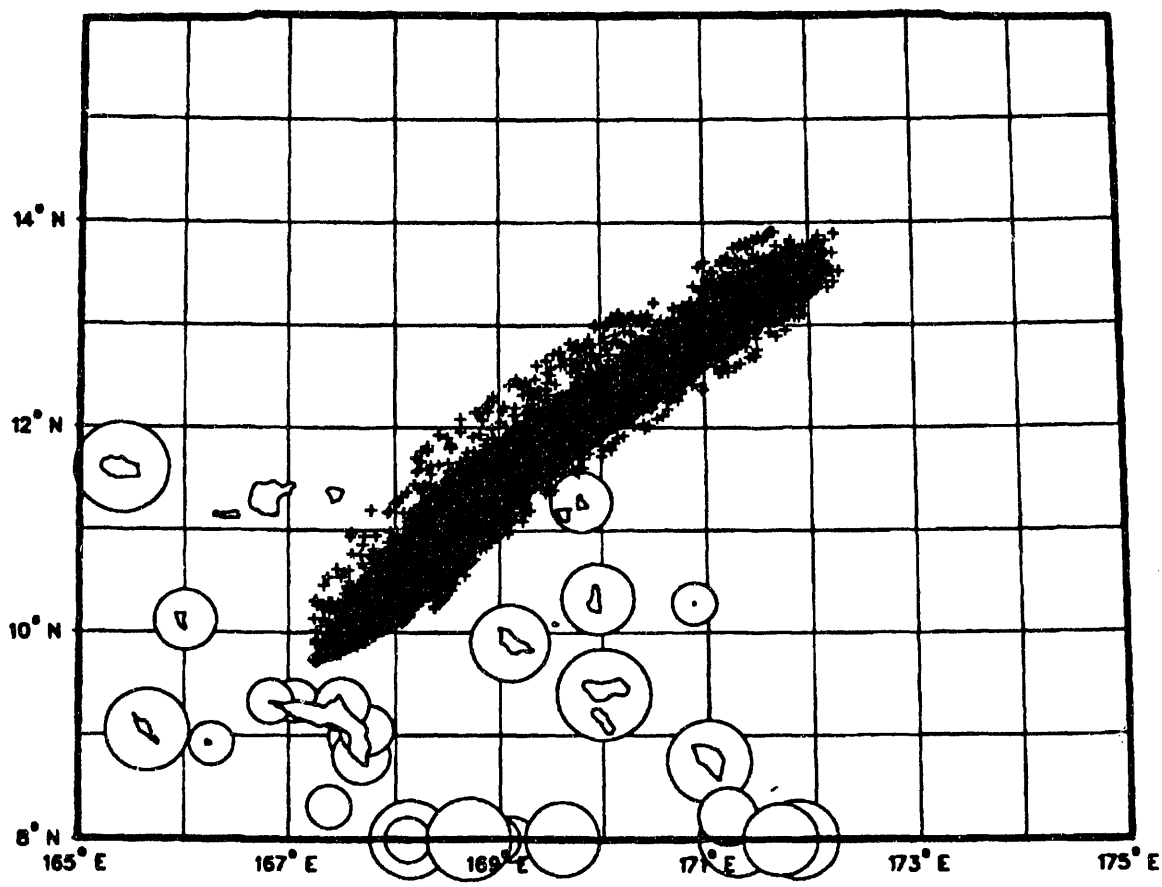

Figure 11: Hard Over Nozzle Tumble Turn Failure Mode
With Initial State Covariance Matrix
and With 3 Second Delay

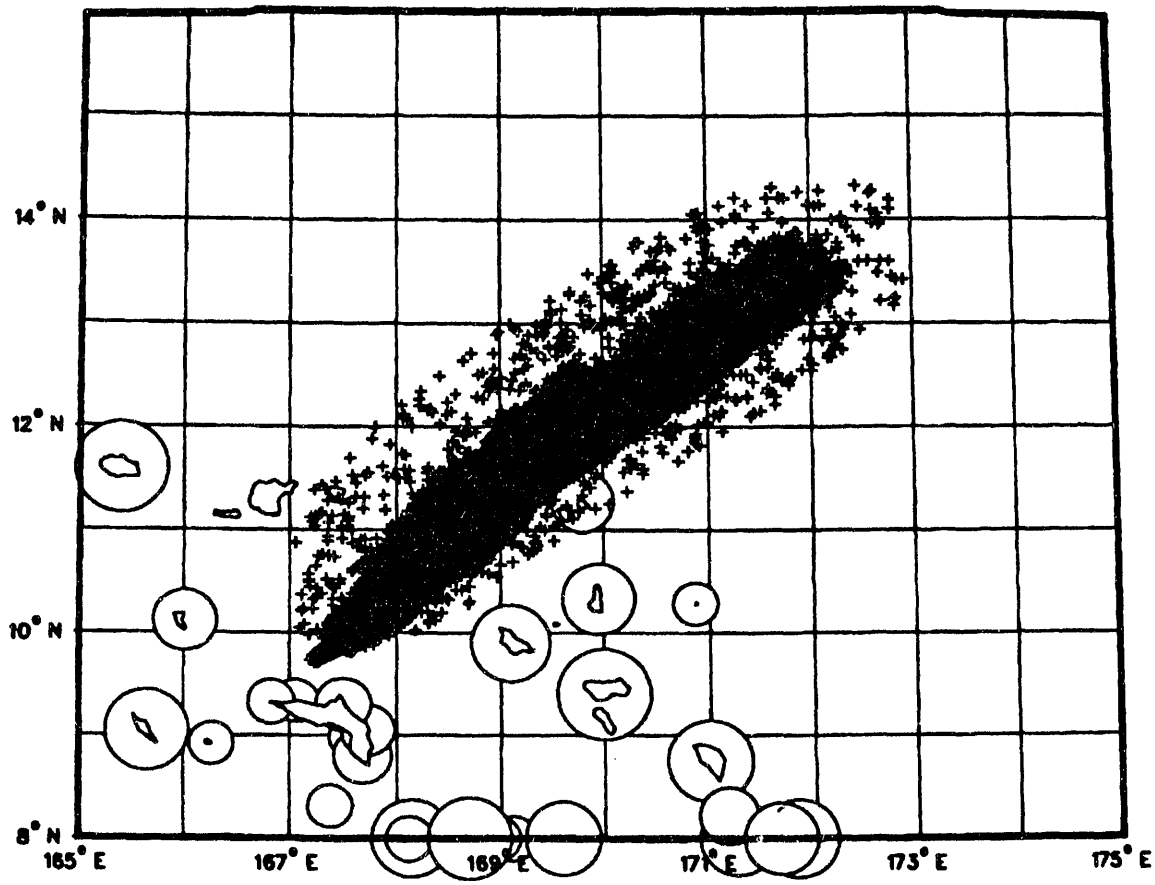

Figure 12: Hard Over Nozzle Tumble Turn Failure Mode
With Initial State Covariance Matrix
and With 4 Second Delay

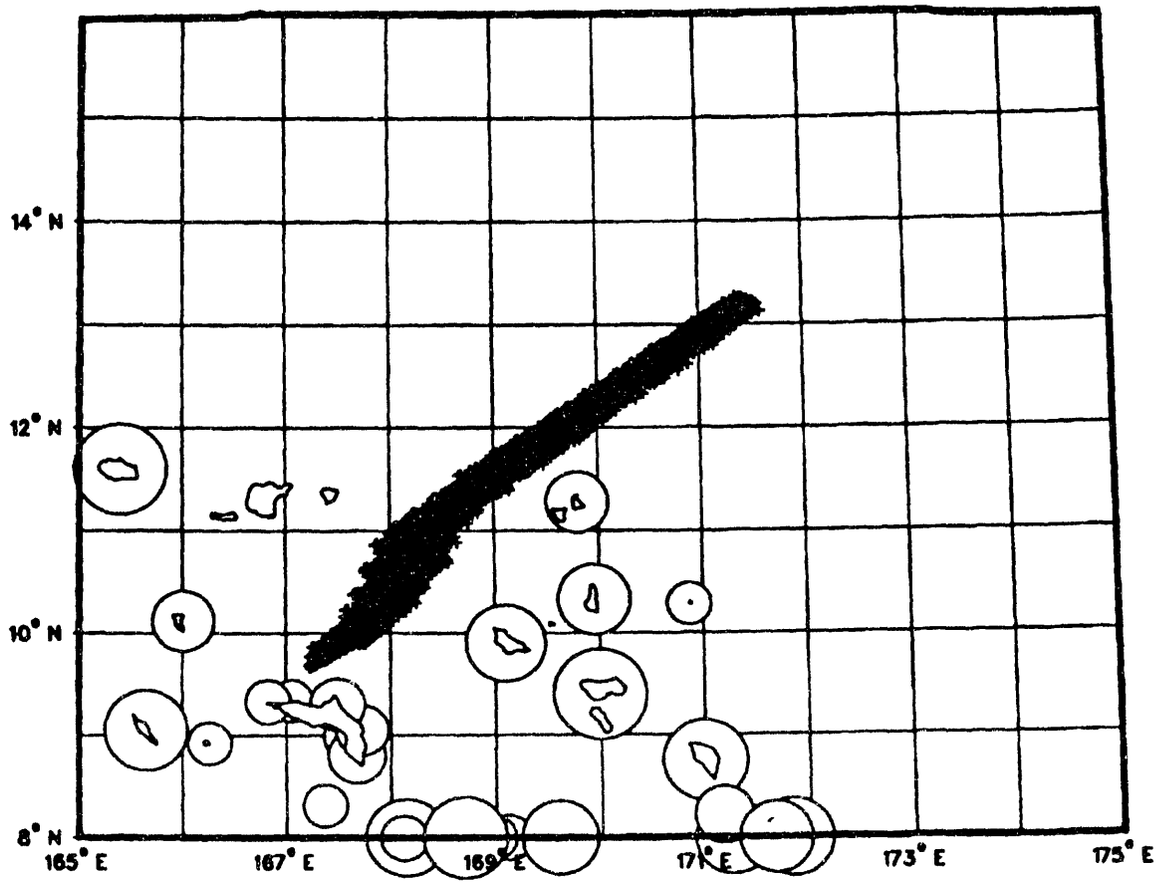

Figure 13: Stuck Nozzle Tumble Turn Failure Mode
With Initial State Covariance Matrix
and With 3 Second Delay

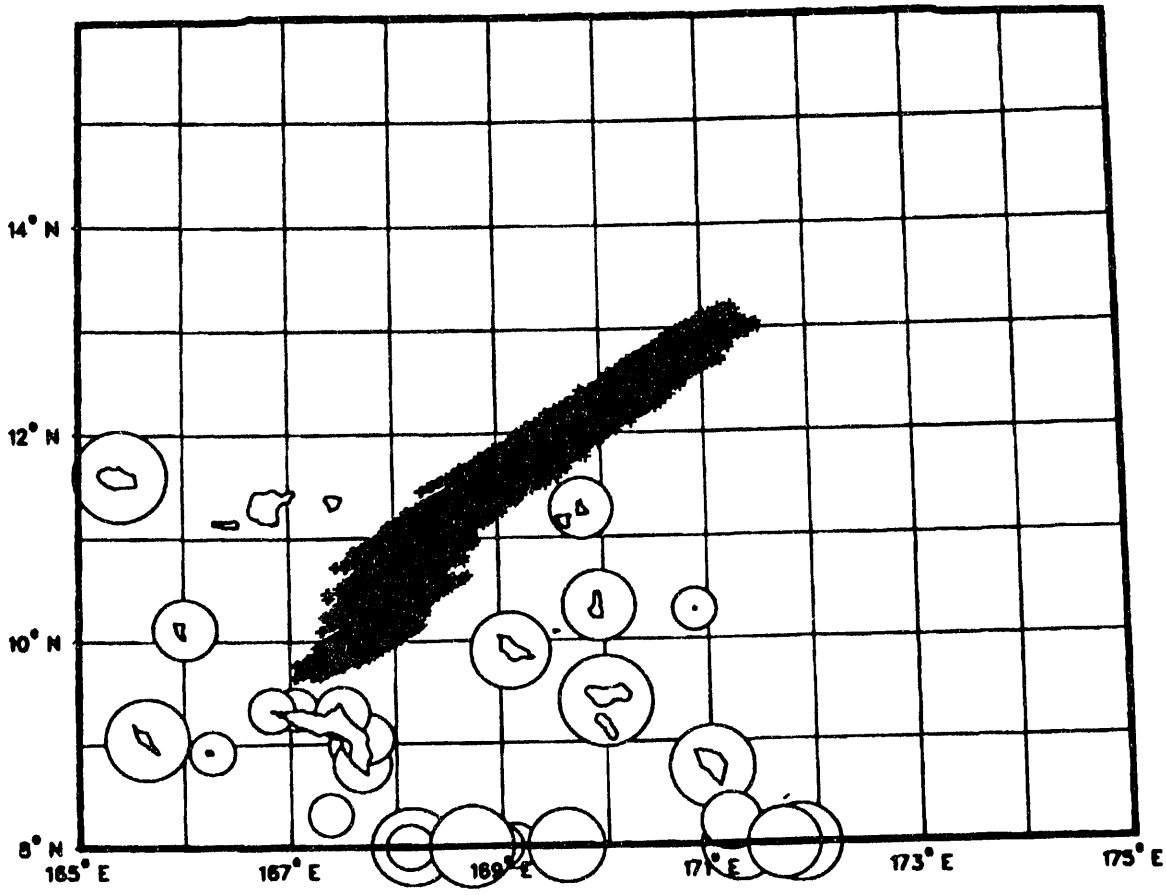

Figure 14: Stuck Nozzle Tumble Turn Failure Mode
With Initial State Covariance Matrix
and With 4 Second Delay

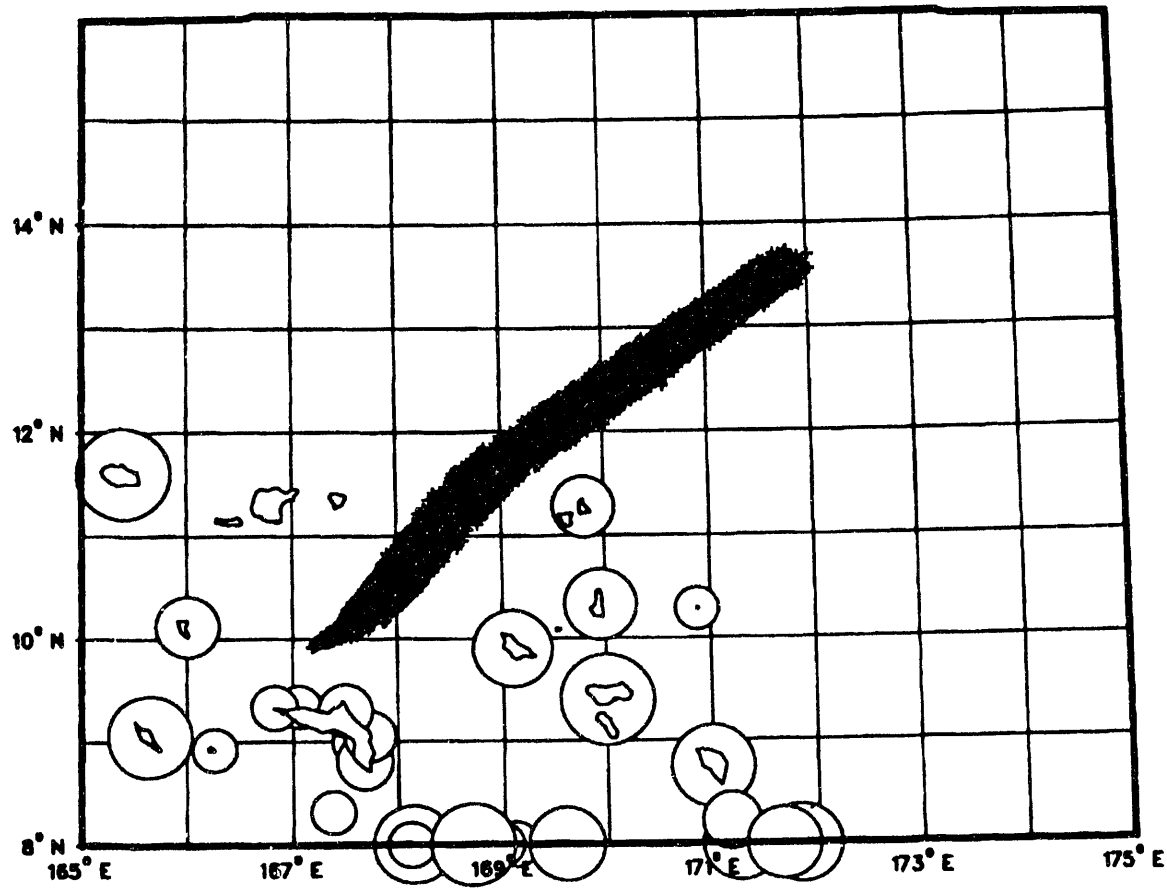

Figure 15: Null Position Nozzle Tumble Turn Failure Mode
With Initial State Covariance Matrix
and With 3 Second Delay

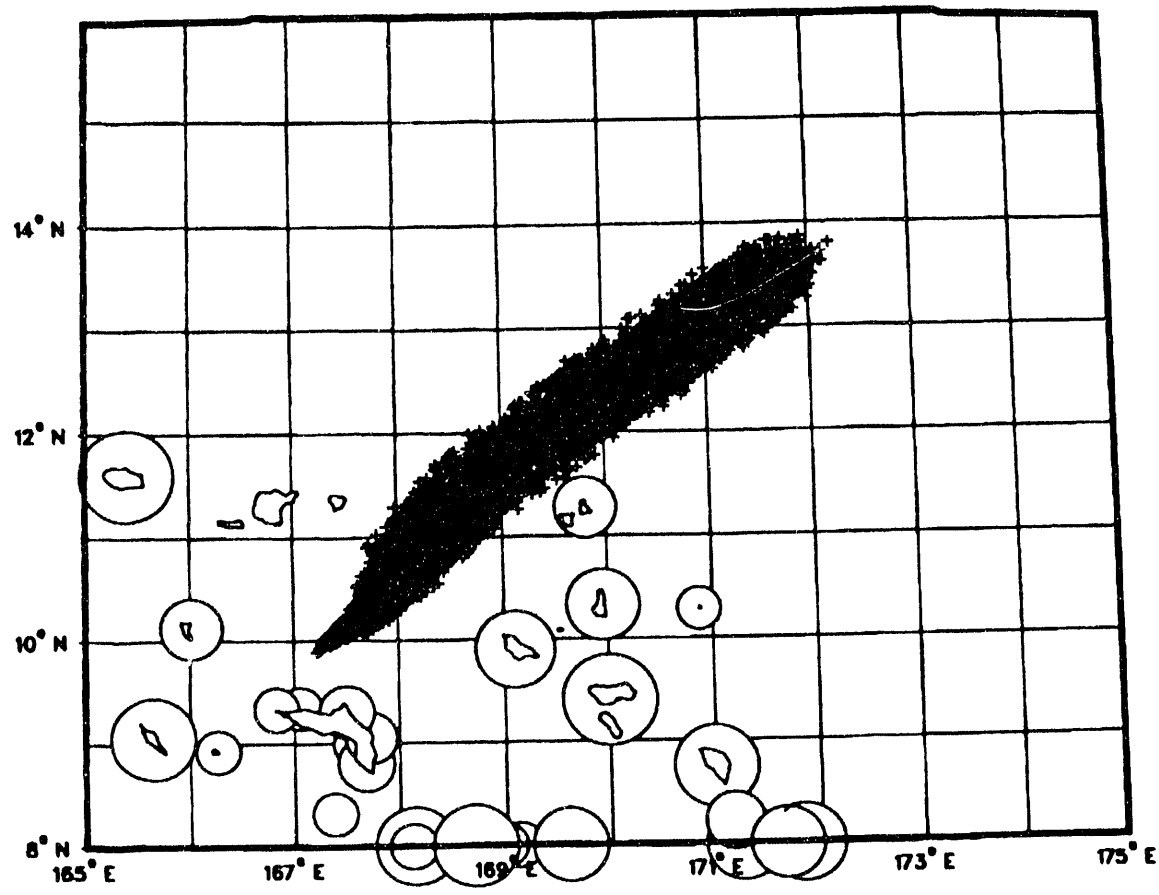

Figure 16: Null Position Nozzle Tumble Turn Failure Mode
With Initial State Covariance Matrix
and With 4 Second Delay

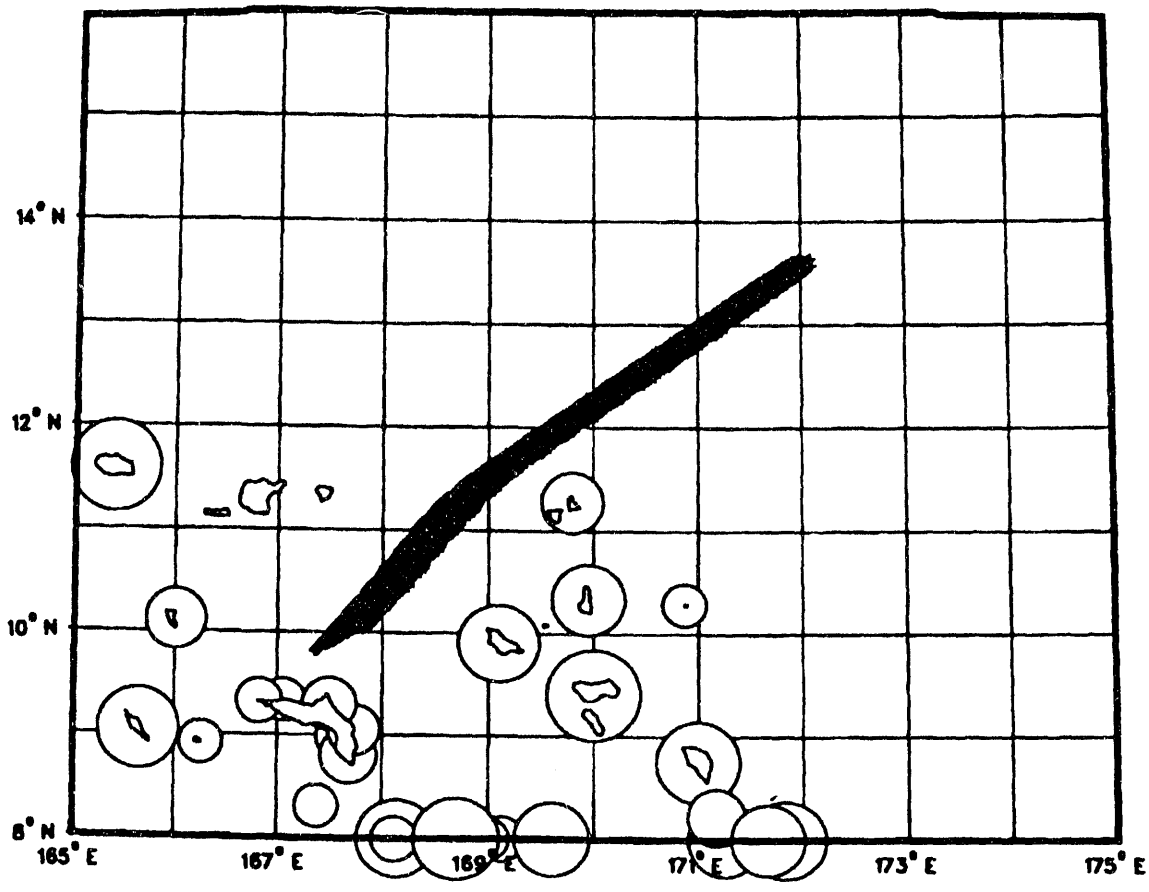

Figure 17: Instantaneous Destruct Failure Mode
With Initial State Covariance Matrix

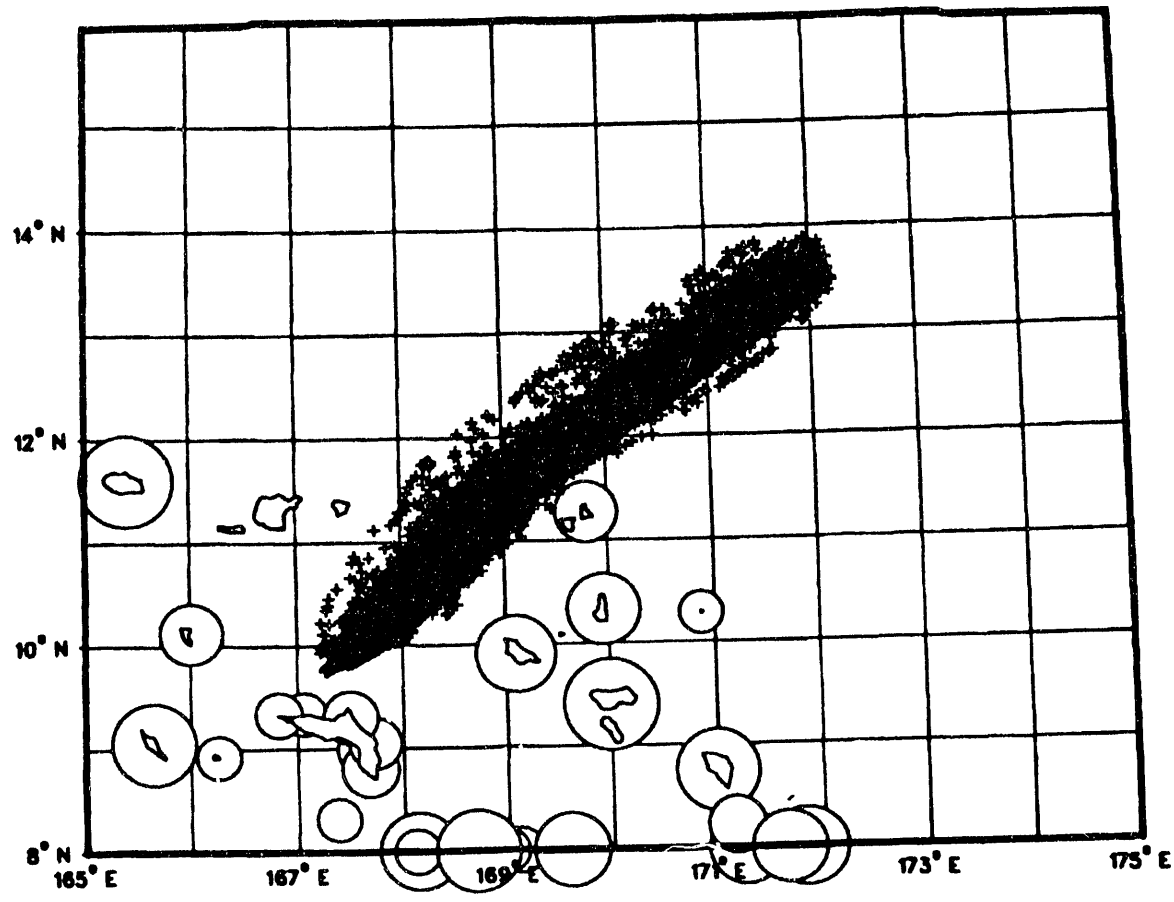

Figure 18: Hard Over Nozzle Tumble Turn Failure Mode
With 3 Second Delay Between Failure on
Nominal Trajectory and FTS Activation

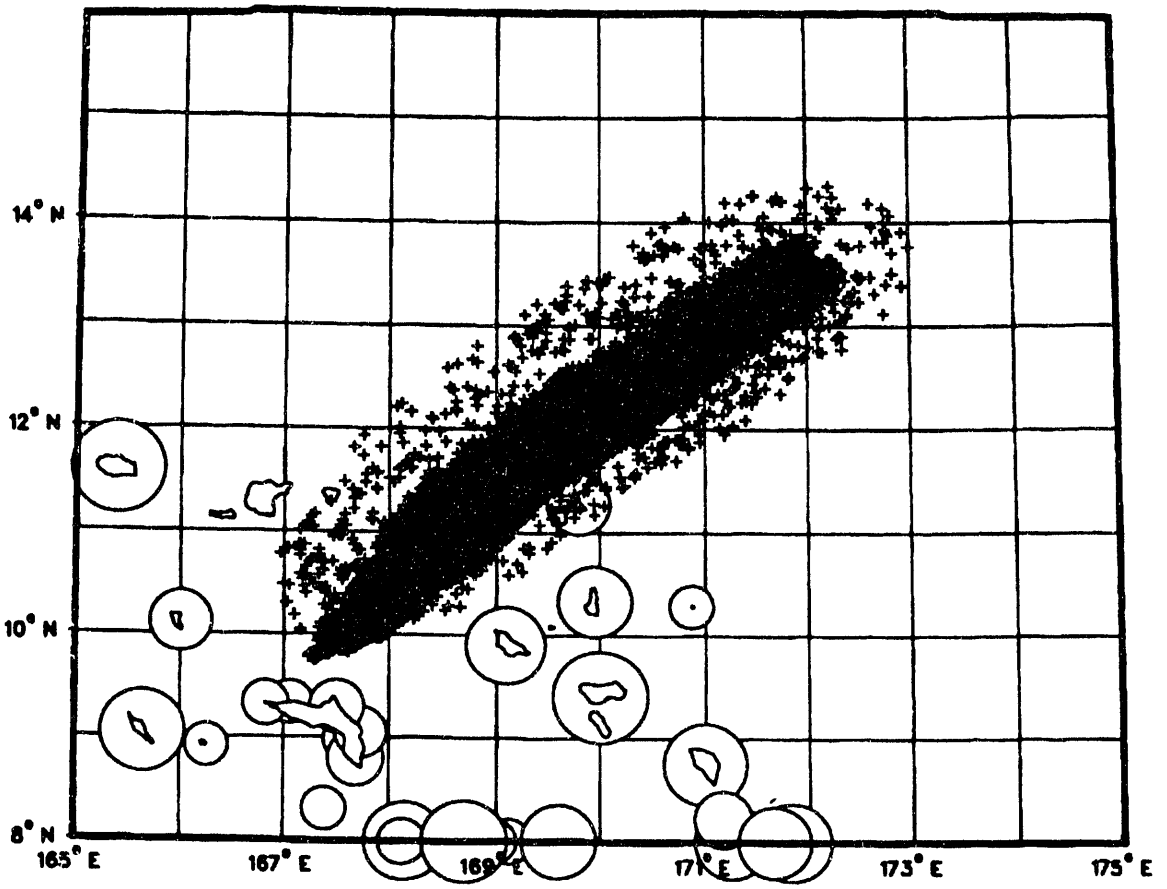

Figure 19: Hard Over Nozzle Tumble Turn Failure Mode
With 4 Second Delay Between Failure on
Nominal Trajectory and FTS Activation

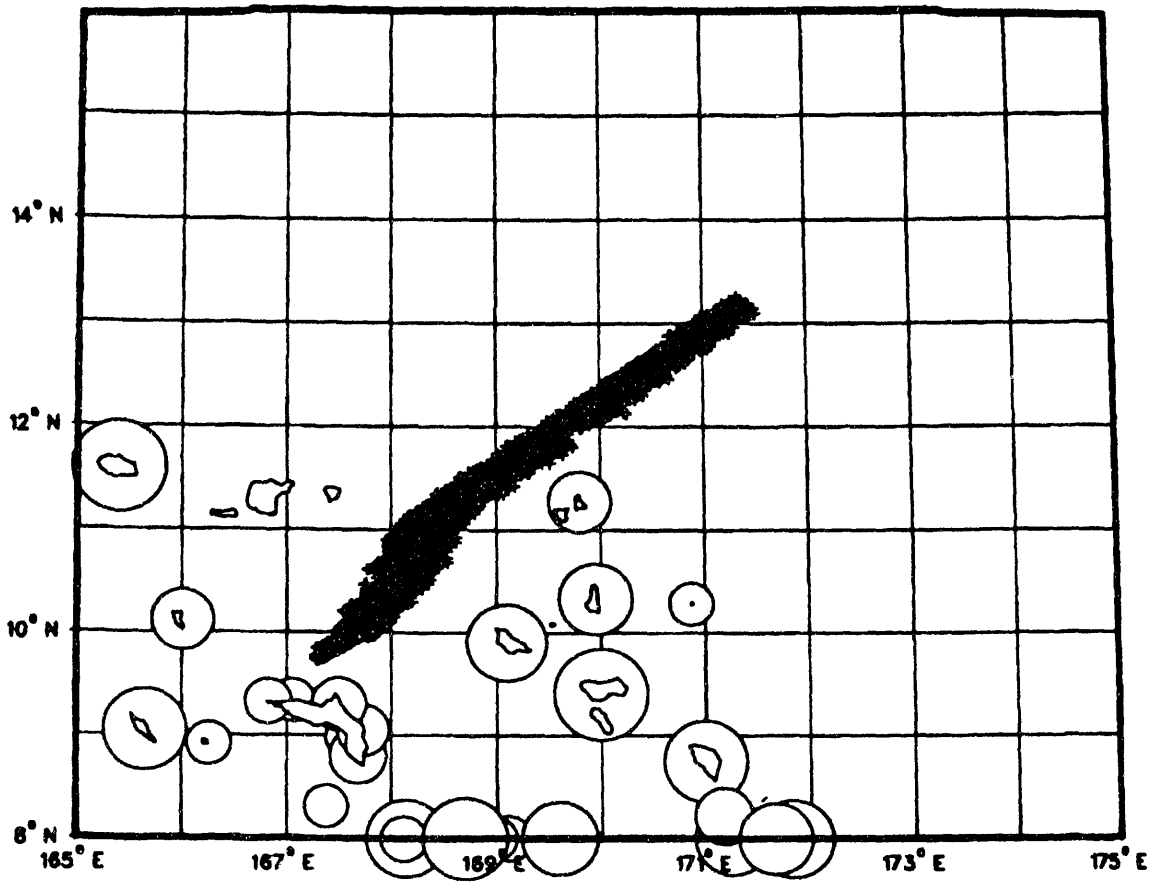

Figure 20: Stuck Nozzle Tumble Turn Failure Mode
With 3 Second Delay Between Failure on
Nominal Trajectory and FTS Activation

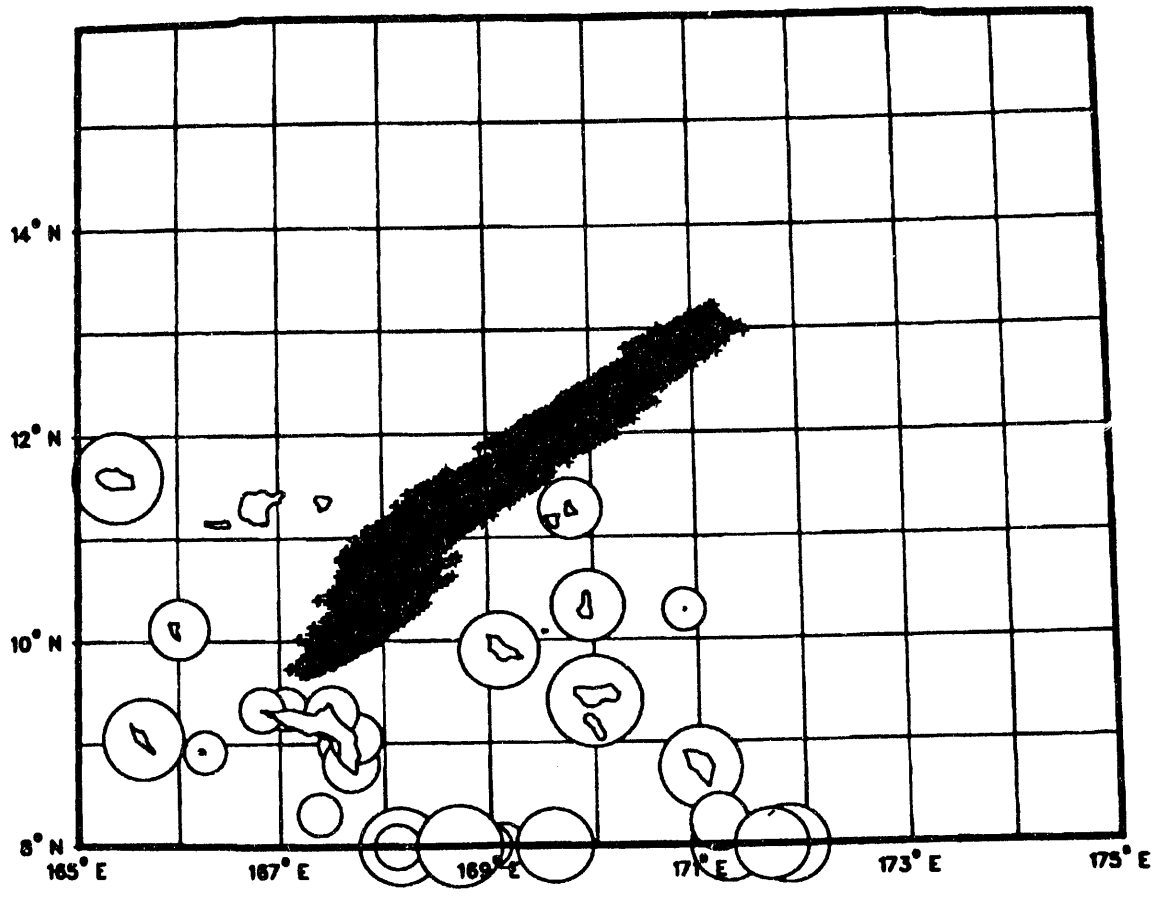

Figure 21: Stuck Nozzle Tumble Turn Failure Mode
With 4 Second Delay Between Failure on
Nominal Trajectory and FTS Activation

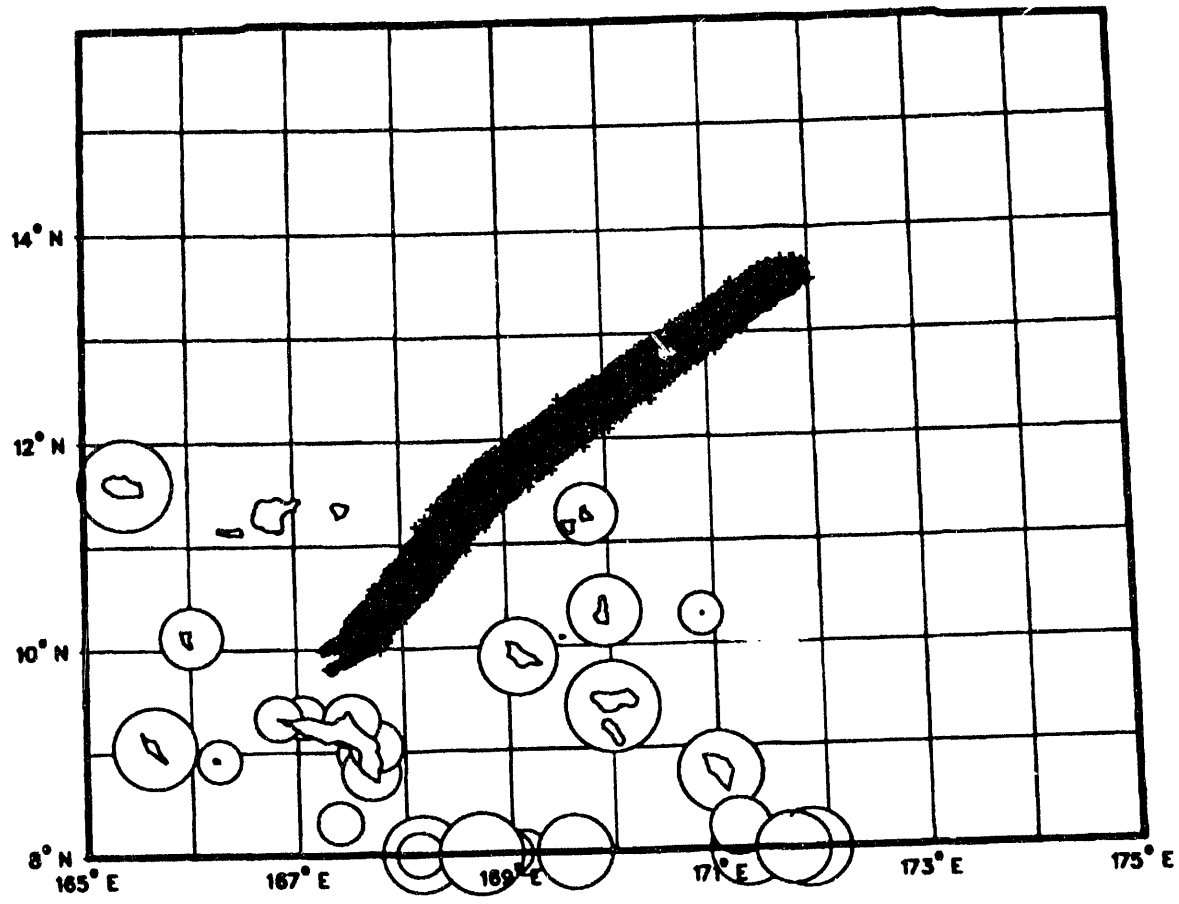

Figure 22: Null Position Nozzle Tumble Turn Failure Mode
With 3 Second Delay Between Failure on
Nominal Trajectory and FTS Activation

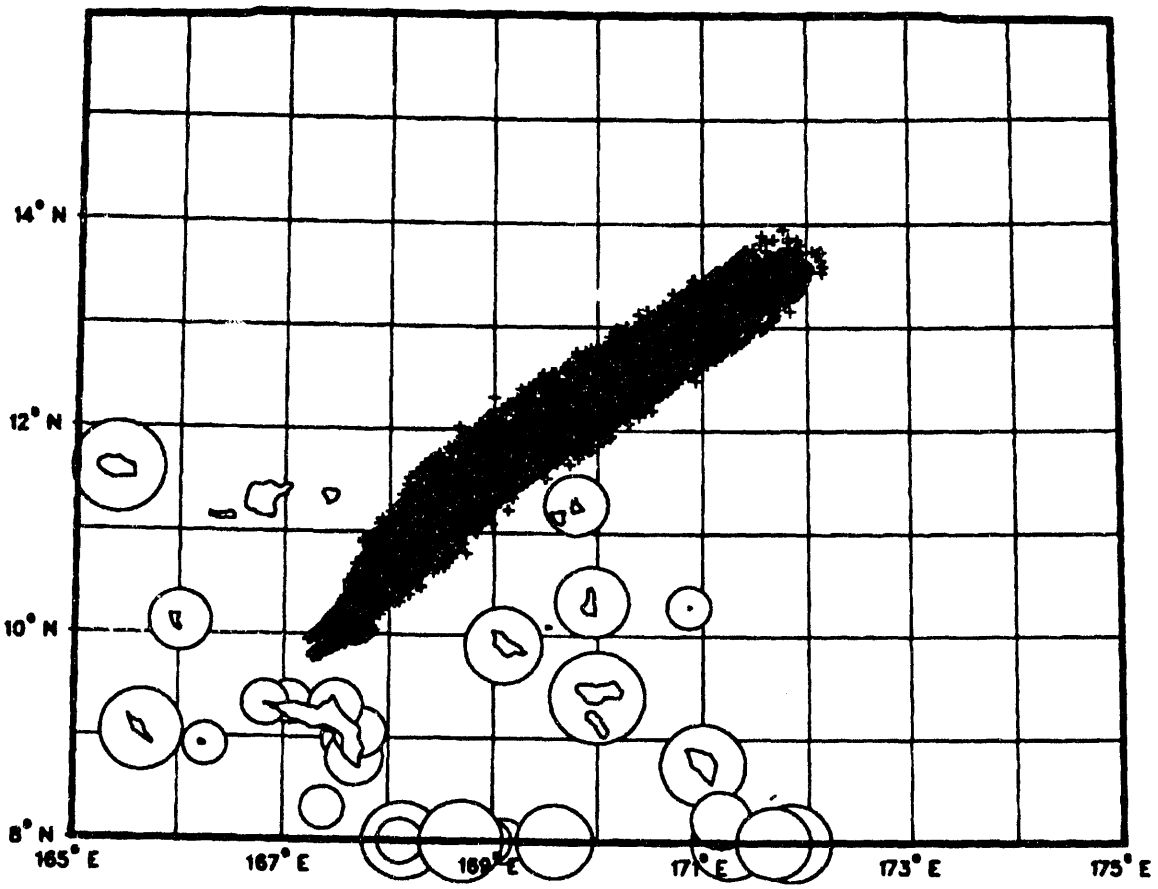

Figure 23: Null Position Nozzle Tumble Turn Failure Mode
With 4 Second Delay Between Failure on
Nominal Trajectory and FTS Activation

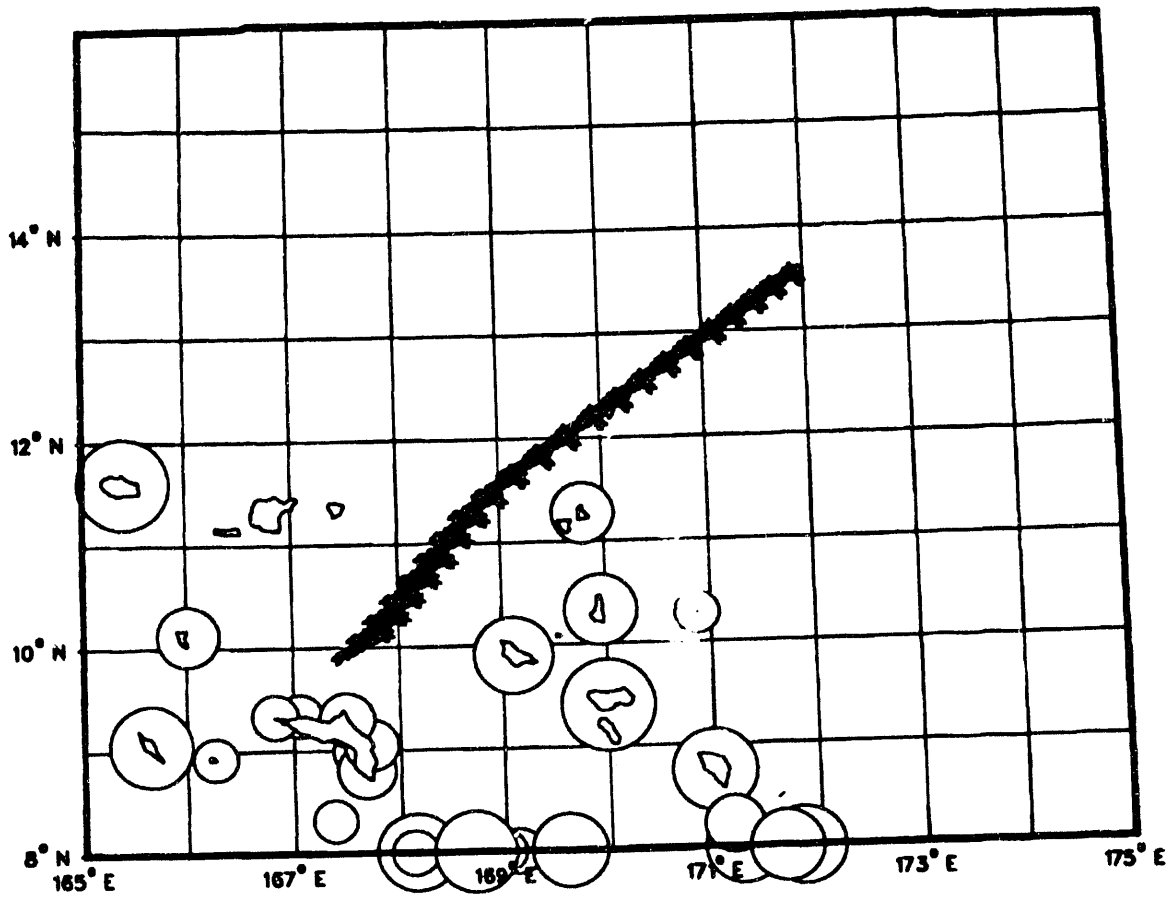

Figure 24: Instantaneous Destruct Failure Mode
on Nominal Trajectory

Distribution

External Distribution

1. Jack McCreary
   USA SSDC
   STARS Product Office
   P. O. Box 1500
   Huntsville, AL 35807 - 3801

2. Irene Hofer
   NAWC WPNS
   Safety Office, Code P3411
   Pt. Mugu, CA 93042

3. Aubrey Kunishige
   Pacific Missile Range Facility
   Code 7332F
   Barking Sands, HI 96752 - 0128

4. Robert Valencia
   KMR Safety Office
   USAKA CSSD - KA - RS
   P. O. Box 26
   APO San Francisco, CA 96555 - 2526

5. Russell George
   Tybrin Corporation
   4900 University Square, Suite 28
   Huntsville, AL 35807

Internal Distribution

6.	1500	David J. McCloskey
7.	1501	Carl W. Peterson route to: 1512, 1513, 1552
8.	1502	Paul J. Hommert route to: 1511, 1553, 1554
9.	1551	Walter P. Wolfe
10.	1551	Kenneth V. Chavez
11.	1551	J. Kenneth Cole
12.	1551	Teresa M. Jordan
13.	1551	Marc W. Kniskern
14.	1551	Robert A. LaFarge
15.	1551	William A. Millard
16.	1551	David E. Outka (5)
17.	1551	Larry W. Young
18.	1561	Harold S. Morgan route to: 1562
19.	2723	Richard G. Hay
20.	2723	Alonzo A. Lopez
21.	2725	Eric J. Schindwolf
22.	2725	Margaret R. Weber
23.	7141	Technical Library (5)
24.	7151	Technical Publications
25.	7613-2	Document Processing for DOE/OSTI (10)
26.	8523	Central Technical Files
27.	9101	Alfred C. Watts
28.	9132	Rance S. Edmunds
29.	9132	John E. White

DATE
FILMED
12/14/93
END